CHALMERS

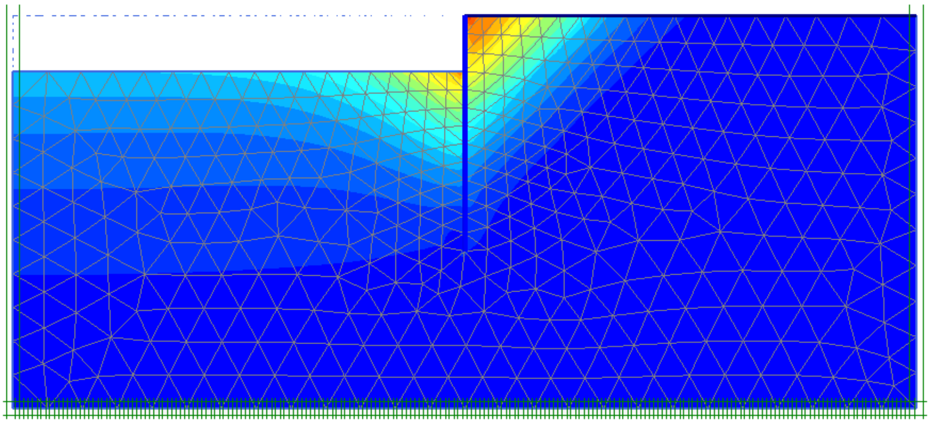

Modelling of an Excavation in Sensitive Soil with Strain Rate Dependency

Master of Science Thesis in the Master's Programme Infrastructure and Environmental Engineering

JOSEFIN PERSSON

Department of Civil and Environmental Engineering
Division of GeoEngineering

Geotechnical Engineering Research Group

CHALMERS UNIVERSITY OF TECHNOLOGY
Göteborg, Sweden 2013

Master's Thesis 2013:42

MASTER'S THESIS 2013:42

Modelling of an Excavation in Sensitive Soil with Strain Rate Dependency

Master of Science Thesis in the Master's Programme

JOSEFIN PERSSON

Department of Civil and Environmental Engineering
Division of GeoEngineering
Geotechnical Engineering Research Group
CHALMERS UNIVERSITY OF TECHNOLOGY

Göteborg, Sweden 2013

Modelling of an Excavation in Sensitive Soil with Strain Rate Dependency

Master of Science Thesis in the Master's Programme
JOSEFIN PERSSON

Examensarbete / Institutionen för bygg- och miljöteknik,
Chalmers tekniska högskola 2013:42

Department of Civil and Environmental Engineering
Division of GeoEngineering
Geotechnical Engineering Research Group
Chalmers University of Technology
SE-412 96 Göteborg
Sweden
Telephone: + 46 (0)31-772 1000

Cover:
Graph showing deformation generated by an excavation with safety factor of 1.5 and creep.

Department of Civil and Environmental Engineering
Göteborg, Sweden 2013

Modelling of an Excavation in Sensitive Soil with Strain Rate Dependency
Master of Science Thesis in the Master's Programme

JOSEFIN PERSSON
Department of Civil and Environmental Engineering
Division of GeoEngineering
Geotechnical Engineering Research Group
Chalmers University of Technology

ABSTRACT

Due to urbanisation cities are becoming more populated every day. These cities are often located in river valleys with soft sensitive soil not suitable for construction. These soils exhibit anisotropic behaviour as well as destructuration and development of creep strains with time. Prediction of soil behaviour for these is problematic and research is currently being conducted into different modelling techniques to obtain more realistic results.

Two different material models been analysed in this thesis. The Hardening soil model is used as reference and Creep-SCLAY1S is used to investigate the strain rate in soil close to an excavation. Both these models are used in the finite element program PLAXIS where Creep-SCLAY1S is a user defined model that was introduced in 2012.

Three cases have been used to investigate the behaviour of creep in clay as simulated by Creep-SCLAY1S. The first case is a shallow excavation with a train loads next to it simulated to see how the dynamic train load influence the stability of the excavation over time. The second case is a deeper excavation without the train load. The focus in this case is to predict how long the excavation can stand until the clay reaches creep rupture but also to show how this corresponds to the global factor of safety. The third case is a simulation of undrained triaxial compression tests with creep which to investigate when tertiary creep occur in the soil specimen.

The dynamic case showed unrealistic results and further research on the rate dependent model and its use in ultimate limit state is recommended. The results from the second and third case show that creep rupture occur earlier for lower factors of safety but also that the time the excavation can stand is uncertain due to sensitivity to several input parameters for the model.

It has been shown that Creep-SCLAY1S models the behaviour of creep rupture well at an excavation for serviceability states. However, it has also been shown that the model is not capable for ultimate limit states. The results indicate that there is a need for a margin in the factor of safety, to ensure that there is no creep rupture at the excavation as the creep develops over time. Further research and parametric studies of Creep-SCLAY1S is recommended before it is implemented as an everyday tool to analyse rate effects at excavations.

Key words: Anisotropy, Creep, Creep-SCLAY1S, Destructuration, Excavation, Hardening Soil model, Rate-effect, Sensitive soil

Contents

ABSTRACT V

CONTENTS VII

PREFACE IX

NOTATIONS X

1 INTRODUCTION 1

1.1 Aim 1

1.2 Scope of work 1

1.3 Method 2

1.4 Limitations 2

2 BEHAVIOUR OF SOFT SOIL 3

2.1 Structures and destructuration 3

2.2 Anisotropy 4

2.3 Creep/time-dependency 5

2.4 Failure criteria 5

2.5 Yield envelope 7

2.6 Creep rupture 7

3 STRESS- STRAIN RELATIONSHIPS 11

3.1.1 Elasticity 11

3.1.2 Anisotropic elasticity 12

3.1.3 Elasto-plastic 12

3.1.4 Elastic visco-plasticity 13

4 EXCAVATIONS 14

4.1 Behaviour of soft soil close to an excavation 14

4.1.1 Stress paths 14

4.1.2 Stress paths at an excavation 16

5 LABORATORY TEST 18

5.1 Oedometer test 18

5.2 Triaxial test 19

6 MODELS FOR SIMULATING BEHAVIOUR OF SOFT SOILS 21

6.1 Critical state concept of soils 21

6.2 Hardening soil model 23

6.3 Creep-SCLAY1S 27

7 INPUT PARAMETERS FOR THE MODELS 31
7.1 Parameters for the Hardening soil model 31
7.1.1 Modified parameters for the Hardening Soil model 33
7.2 Parameters for the Creep S-CLAY1S model 36
7.2.1 Modified parameters for the Creep-SCLAY1S model 39

8 MODELLING OF CASE 43
8.1 Case 1 – Excavation with train load 43
8.1.1 Geometry 44
8.1.2 Calculation 46
8.2 Case 2 – Excavation without train load 47
8.2.1 Hardening soil model 48
8.2.2 Creep and parametric study 49
8.2.3 Comparison of Hardening soil model and Creep-SCLAY1S 56
8.3 Case 3 – Creep in Triaxial Compression Tests 58

9 DISCUSSION 61
9.1 The Hardening Soil model 61
9.2 Creep-SCLAY1S 62
9.3 Case 1 62
9.4 Case 2 63
9.5 Case 3 64

10 CONCLUSION 65

11 REFERENCES 66

12 APPENDICES 69

Preface

This thesis has been performed from January to June 2013 at the Department of Infrastructure and Environmental Engineering at Chalmers University of Technology in collaboration with Skanska Teknik and Skanska Grundläggning. The project was conducted at the research group GeoEngineering.

I would like to thank my two supervisors Anders Kullingsjö and Torbjörn Edstam for their help during this project. Anders has provided much support and knowledge in the subject and Torbjörn has always been ready with new ideas and ways to approach problems. I would also like to thank Mats Olsson at Chalmers University of Technology for providing additional laboratory test.

Many thanks also to Patrik Andersson at Skanska Grundläggning for his endless support during the initial stages of this thesis.

Finally, I would like to thank Minna Karstunen at Chalmers University of Technology. She has committed many hours to helping me during this project, both assisting me with the modelling, the report and other issues. In addition, I would like to especially thank her for the private lectures on the, to me, new material she held in the beginning of the project.

Göteborg, June 2013

Josefin Persson

Notations

Roman upper case letters

E	Young's modulus
E_{50}	plastic cone hardening secant modulus
E_{oed}	plastic cap hardening secant modulus
E_{ur}	elastic unloading tangent modulus
G	shear modulus
K	bulk modulus
K_0	lateral earth pressure at rest
K_0^{nc}	K0 value for normal consolidation
M	Critical failure line
M	Oedometer modulus
M'	modulus number
M_0	Constant constraint modulus below effective vertical preconsolidation pressure
M_L	Constant constrained modulus between vertical preconsolidation pressure and σ'_L
Rf	failure ratio (Hardening soil model)
S	vector for plastic strains

Roman lower case letters

c'	apparent cohesion
e_0	initial void ratio
m	power for stress level dependency
p'	total mean effective stress
p^{ref}	reference value
q	deviatoric stress
s'	average value of σ_1 and σ_3 in the axial symmetric case
t'	difference between σ_1 and σ_3 divided by two in the axial symmetric case
u	pore pressure
v	specific volume
w_L	liquid limit
v_κ	intercept on unloading reloading line
v_λ	intercept on normal compression line

Greek letters

Γ	location of critical state line in compression plane
α_0	Initial inclination of the yield surface
γ	unit weigth of soil
ε	normal strain
ε^e	elastic strain
ε^p	plastic strain
ε_q	deviatoric strain
ε_q^p	plastic shear strain
ε_v	volumetric strain
ε^{vp}	visco-plastic strain
ε_v^p	plastic volumetric strain
η	stress ratio q/p'
κ	slope of unloading reloading line in v:lnp' plane
κ*	slope of swelling/recompression line in e:lnp' space
λ	Slope of normal compression line in v:lnp' plane
λ*	slope of post yield compression line in e:lnp' space for reconstituted samples
λi*	slope of post yield compression line in e:lnp' space for reconstituted samples
μ*	modified creep index
ν	poisson’s ratio
ν_{ur}	poisson’s ratio for unloading/reloading
ξ	absolute rate of destructuration
ξd	relative rate of destructuration
σ	normal stress
σ’	effective stress
σ'_h	horizontal effective stress
σ'_v	vertical effective stress
σ_1	major principle stress
σ_2	intermidiate principle stress
σ_3	minor principle stress
τ	shear stress
τ	reference time
φ	friction angle for a material
χ_0	Initial bonding

ψ	dilation angle
ω	absolute effectiveness of rotational hardening
ω_d	relative effectiveness of rotational hardening

Abbreviations

CK_0UC	K_0 consolidated samples compressed to failure in a triaxial test under undrained conditions
CK_0UE	K_0 consolidated samples extended to failure in a triaxial test under undrained conditions
DSS	direct simple shear test
nrl	normal compression line
OCR	overconsolidation ratio
POP	Preoverburden pressure
url	unloading reloading line

1 Introduction

Urban areas are becoming more congested due to urbanisation. People move from the country into cities and these areas become more densely populated. Because of this regions with soft soil that were considered too unstable for construction just recently are now becoming populated and construction of infrastructure and buildings become necessary. Construction on soft soil is a challenge in geotechnical engineering and a lot of research is conducted on different modelling techniques to obtain more realistic results.

Finite element modelling has been used in geotechnical engineering for many years. The first comprehensive constitutive model, Cam Clay, was presented by Schoefield and Roscoe in 1963 and modified by Roscoe and Burland in 1968. Research has continued to make more realistic models, especially to capture the stress-strain behaviour of the clay. The latest approaches to improve on these models have mainly been focused on three key features; anisotropy, destructuration and time-dependency or creep (Wheeler et al. 2003). One of the new models, Creep-SCLAY1S, capturing all three effects will be used in this thesis to model rate dependent behaviour of sensitive clay.

Skanska is a construction company operating in Sweden. It is a large company with many divisions. One of these divisions is Skanska Teknik which design structures before construction. One type of structures is temporary excavations. When constructing these in soft soil creep develops in the clay. This creep influences the stability of the temporary excavation and it is important to investigate how long an excavation can be open before if fails due to creep or has to low stability. Creep-SCLAY1S will used to investigate this behaviour in an excavation.

1.1 Aim

The aim of this thesis is to model the deformation in sensitive clay close by and around an excavation, and also to investigate how long time it takes for the soil to reach failure in an open cut. The problem will be solved by using finite element analysis.

1.2 Scope of work

The work with this thesis will be carried out in different stages to meet the objectives.

- Literature studies about critical state soil mechanics, constitutive models, anisotropy and destructuration.
- Understanding several advanced soil models and the development of the latest and most advanced models.
- In depth investigations of the performance of two models by simulating three cases and by comparing the result with each other. The two models that will be further investigated are the Hardening Soil model and Creep-SCLAY1S.
- Discussion about the advantages and drawbacks, of the two models and how they work in practice.

1.3 Method

The study will be performed using the finite element program, PLAXIS 2D. Two constitutive models are going to be used for modeling the viscous behavior of a soil at an excavation. The material models for the excavation will be the Hardening Soil model and a recently developed soft soil model that accounts for the rate effects of anisotropic soils. These models are constitutive models that are implemented or standard in PLAXIS user defined models. The investigated excavation will be taken from an already finished railway profile and the input data for the model will be derived based on triaxial tests which will be provided by Skanska.

1.4 Limitations

The project will not be modelled in PLAXIS 3D and no other model alternatives, like multilaminate models, will be used for modelling the anisotropic behaviour of the clay. Only compressive strength will be used in the modelling phase.

2 Behaviour of soft soil

The behaviour of soft soil is influenced by several factors. First three key features for the models will be explained and the next section of this chapter will explain constitutive behaviour of a soil which is a basic feature for all models.

2.1 Structures and destructuration

Burland (1990) presented a new concept on how to describe a natural soil, Burland defined the natural soil as a "structure" which consists of two parts. The first part was named fabric which is the spatial arrangement of the soil particles, particle groups and pore spaces. The second part was the bonding between the particles.

The term destructuration, was presented by Leroueil et al. (1979), and describes the damage that these bonding are affected by plastic straining. This was shown by Burland 1990 when he displayed results from two compression tests on the same type of soil but one of the soil specimens had been reconstituted. The different results of the test were explained with destructuration of bonding between the particles. Similar test has been performed on Rosmére clay, see figure 2.1, the clay in this test has been compressed under triaxial loading. The hatched area in the figure displays the influence of structure. It is possible to see that the structure gives additional strength and stiffness to the soil skeleton (Hinchberger et. al 2010) and it can be seen that destructuration leads to softer response in the soil than before (Grimstad et al. 2010).

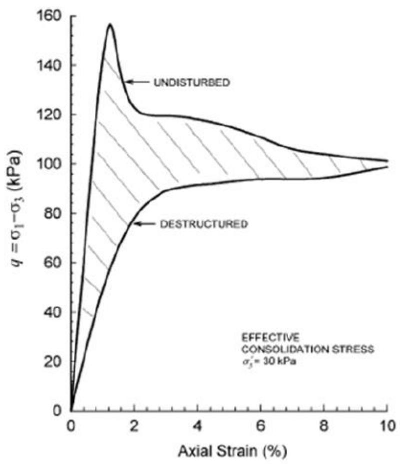

Figure 2.1 Stress strain response for structured and destructured Rosemére clay in triaxial compression (Lefebvre, 1981).

Figure 2.2 shows the difference in behaviour for a reconstituted sample and natural soil in an oedometric loading test. In this schematic figure all influence from anisotropy are ignored. The reconstituted soil would follow an intrinsic compression line while the natural soil, which has initial bonding from the beginning, would yield at the elevated value of the effective stress and later on meet with the intrinsic compression line when the bonding was destroyed (Wheeler et. al, 2003)

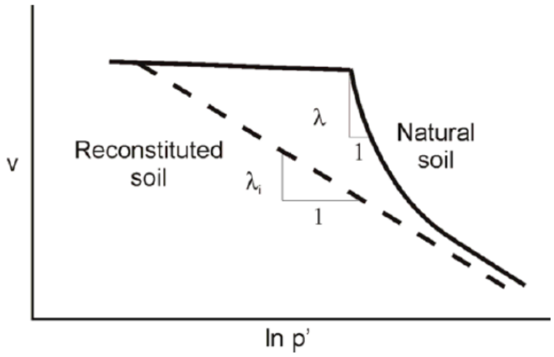

Figure 2.2 Influence of destructuration during oedometric loading (Wheeler et al. 2003).

2.2 Anisotropy

Natural or slightly overconsolidated soft clay tends to have an anisotropic fabric due to its deposition and one-dimensional consolidation. During this deposition the clay has become compressed in a vertical direction but constrained in the horizontal direction. If a soil is affected by plastic strains there can be a re-orientation of particles and changes in the particle contacts which may lead to change in anisotropy in the clay.

The anisotropy in the clay affects both the elastic and plastic stress-strain behaviour. In this thesis only normally or slightly overconsolidated clays are investigated and in this kind of clay the plastic deformations are dominant compared to the elastic strains. The plastic strains are due to that of more importance then the elastic strains (Wheeler et. al, 2003).

Investigation of plastic anisotropy in soils shows that it has great effect on the soils strength and stiffness, see Figure 2.3. The figure shows the stress-strain curves for Gloucester clay from undrained triaxial compression tests. The different curves represent a different angle that the soil is collected from. The results of the different shear strengths and stiffness in the figure are explained by the anisotropy of soil.

Neglecting anisotropy when modelling a geotechnical problem in a finite element program may lead to highly inaccurate predictions of the soil response (Grimstad et. al , 2010).

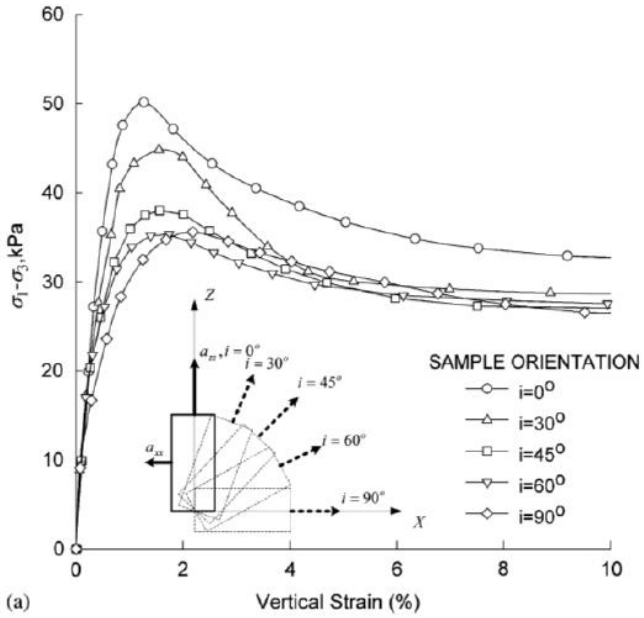

Figure 2.3 Influence of anisotropy on undrained triaxial compression test (Hinchberger, Qu, & Lo, 2010).

2.3 Creep/time-dependency

The behaviour of creep and time dependency behaviour are an important factor when constructing on soft clays. Compression curves, yielding, and undrained shear strength are highly influenced by the rate of straining in the material (Wheeler, et. al 2003). Normally consolidated clays have only been subjected to its own weight and have a high compressibility. When a soft soil is subjected to a load there will be a primary consolidation that is controlled by the soils permeability. This consolidation will make a change in volume due to a decrease in excessive pore water pressure. This kind of consolidation will proceed until the pore pressure is in equilibrium. The secondary consolidation is called creep, and is also a time dependent volume change that is not controlled by the permeability of the soil. This kind of consolidation is slower than the primary consolidation and is ongoing at all time from the change of stress state, even when the primary consolidation is occurring (Sällfors & Andréasson, 1985).

2.4 Failure criteria

An important factor when dealing with geotechnical engineering is the soils shear strength. The shear strength of a soil is described as the amount of shear stress that the soil can withstand without reaching failure and is usually described by Mohr Coulomb's failure criteria. In this criterion the intermediate stress, $\sigma_{2,}$ is neglected and the failure surface is defined by the envelope of Mohr's circles, which are defined by the major and minor principle stresses σ_1 and $\sigma_{3.}$ It can also be defined by the normal stress, σ_n and shear stress τ on the failure plane (Labuz & Zang, 2012).The criterion describes that failure occur when the shears stress τ reaches the critical value of the failure line. See equation 2.1 below.

$$\tau = \pm(c' + \sigma' tan\varphi') \qquad (2.1)$$

where τ is shear stress, σ’ is normal effective stress, c´ is apparent cohesion and φ´ is the frictional resistance of the soil. This means that if sliding is going to occur on any plane the shear stress must be greater than the frictional resistance which is dependent on the effective stress. This equation defines two linear lines in the τ:σ plane and if a Mohr’s circle of effective stress reaches this line, failure occurs (Wood, 1990), see Figure 2.4.

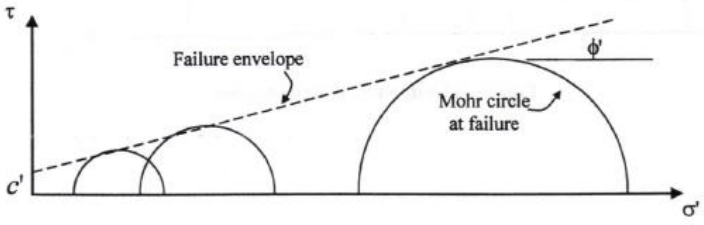

Figure 2.4 Schematic figure over Mohr-Coulombs failure Criteria with Mohr circles and the failure envelope (Wood, 1990).

By selecting the mobilized friction angle to zero, Mohr Coulombs failure criterion reduces to Tresca’s. Tresca’s failure criterion is also called maximum shear stress and is a prism with six sides which have an infinitive length in 3D space. This means that the material is elastic when it is compressed or extended, but if any of the principle stresses becomes larger than the others the material begins to shear.

In the principal stress state the shape of the failure criterion is a hexagonal pyramid and in the π-plane, which is specified by the hydrostatic axis, it is an irregular hexagon (Labuz & Zang, 2012).

Another failure criterion was introduced by Drucker and Prager 1952 who proposed an approximation of Mohr-Coulomb failure criterion, their criterion is a circular cone which touches the corners of Mohr- Coulombs criterion in the three dimensional stress space, see figure 2.5, either in compression or extension.

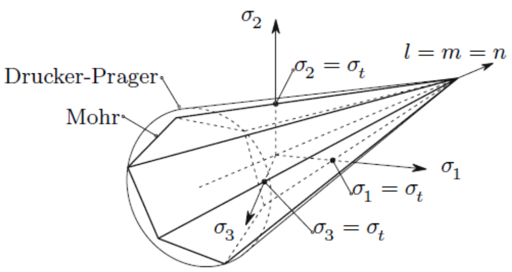

Figure 2.5 Drucker-Prager and Mohr-Coulombs failure criteria’s in principle stress space (Silva, 2006).

The advantage of this failure criterion over Mohr-Coulomb’s is that it does not have any corners and it is hence computationally more stable (Silva, 2006).

Another usual failure criterion is Von Mise's, this is, however, not discussed in this thesis because this criterion is not applied in the models that will be used for this thesis.

2.5 Yield envelope

For a soil that is exposed to stresses higher than the preconsolidation pressure, σ'_p, the soil will undergo large deformations and large strains. If the stress the soil is exposed to is smaller than the preconsolidation pressure the strains will be small. This can be combined with failure criteria to create a yield envelope, see Figure 2.6.

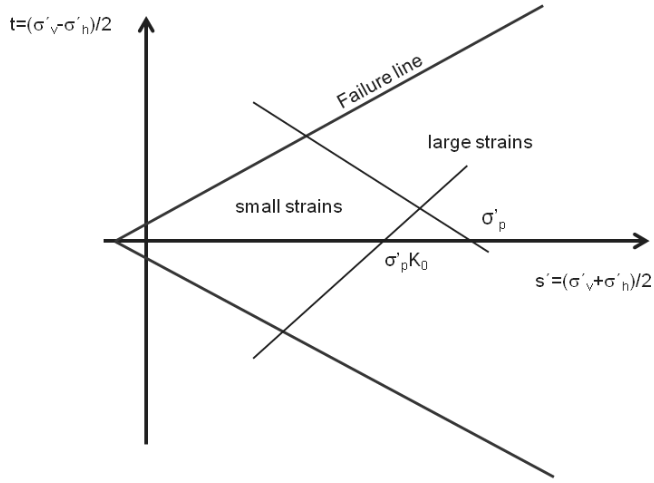

Figure 2.6 Yield envelope with Mohr Coulombs failure criterion.

The failure lines from Mohr coulombs failure criteria for compressive and extension shear strengths restrict the soil in this area. Within the yield envelope the stress is smaller than the preconsolidation pressure σ'_p for the major stress and smaller than $K_0 \cdot \sigma'_p$ for the minor stress, where K_0 is coefficient of earth pressure at rest, see equation 2.2.

$$K_0 = \frac{\sigma'_h}{\sigma'_v} \qquad (2.2)$$

Where σ'_h the effective horizontal is stress and σ'_v is the effective vertical stress. The area that is formed by these lines represents the area were small strains occur, if the relation of the major and minor stress is exceeds large deformations or failure occur. The shape of the yield envelope has more rounded corners than the figure and is depended on several factors like the structure of the clay. (Larsson & Sällfors, 1981).

2.6 Creep rupture

The time dependent behaviour of soil, also called creep was discussed in the beginning of this section. Creep is a deformation that happens to the soil under sustained shearing stresses. At low level of stress the creep may either stop or continue at a subtle after a long time from the ignition of the creep. At higher level off stress an opposite process may occur. The initially creep which could be either steady or slightly decreasing may suddenly start to accelerate and finally end with rupture, see Figure 2.7. This state of creep is called tertiary creep. In conventional soil mechanics this state of a soil has been ignored, however, by ignoring this can lead to excessive deformations which can lead to failure or collapse of structures with time (Campanella & Vaid, 1974).

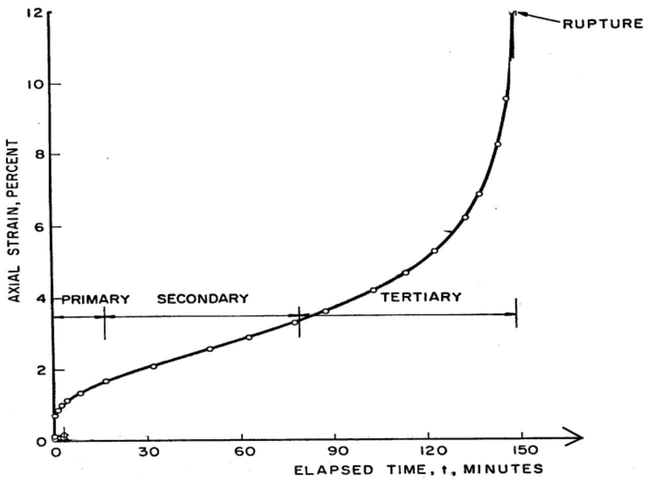

Figure 2.7 Primary, secondary and tertiary creep is shown in the figure with strain in percent over time (Campanella & Vaid, 1974).

The rate of strain has influence over the results of a test when a soil specimen is tested for shearing. This can be divided into two parts, one due to secondary compression and one due to rate effect. This rate effect is described as the energy needed for the water to be pumped into and between pores while shearing. This effect is negligible in sands but in clay it is influencing the test even at very low rate of shearing. Drained triaxial tests are run at very slow strain rates to ensure complete dissipation of pore water in the specimen and the effect of strain rate will be small, while undrained tests are run at higher strain rate and the rate effect will have more influence of the test.

If undrained triaxial tests which are performed with the same strain rate is plotted in a Mohr Coulomb diagram the failure line is a straight line with an intercept on y-axis, see Figure 2.8 .

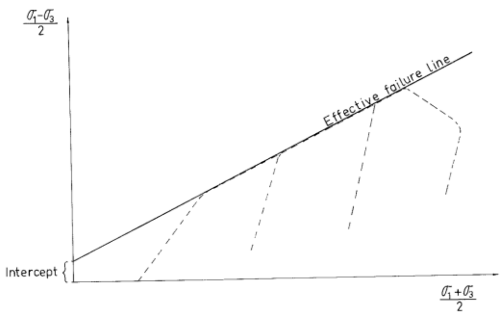

Figure 2.8 Stress paths in undrained triaxial compression tests with equal strain rates (Larsson, 1977).

In Sweden the normal strain rate is 0.6 % per hour and with that rate the intercept is 1-2 kPa. The intercept increases with higher strain rates and disappears at very low rates. This rate effect is only dependent on the permeability of the soil.

In undrained tests with no volume change the secondary compression builds pore pressure in tests that are conducted at slow rates. In the same time as the pore pressure increases the effective mean stress decreases. This increase of pore pressure is dependent on the overconsolidation ratio of the clay just like the secondary compression. Combined rate effects is therefore important in clay with low permeability important.

Larsson (1977) carried on an investigation of creep in undrained tests together with SGI (Swedish geotechnical institute). The tested clay was natural undisturbed clay regarded as typical Swedish clay. The undrained shear stress of the clay was decided before any creep test was carried out. The shear strength of the clay was decided by a shear test at a normal strain rate of 0.6% per hour. The stress paths for this test were plotted, see figure 2.9. The black circle shows failure of the clay.

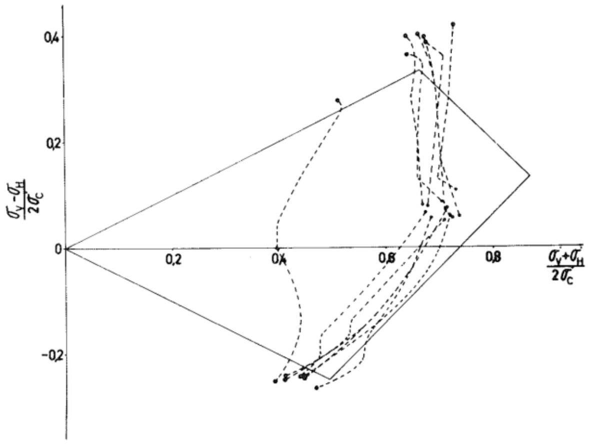

Figure 2.9 Effective stress paths and theoretical yield surface for undrained tests conducted with a strain rate of 0.6% per hour (Larsson, 1977)..

The same clay was in next step tested in creep-series, results from the creep series are shown in Figure 2.10. In the beginning of the creep test the samples were consolidated to in situ stresses. In the next step were the samples subjected to different stress states. The ratio of this new stress state of the soil related to undrained shear strength of the soil determined with regular strain rates is called the degree of mobilization of the clay. From this state of stress all stresses are kept constant with time. In this last step creep can be seen when the stress paths are plotted, see Figure 2.10. If the stress path reaches and passes the failure line during creep the sample will fail, the black circles show failed samples.

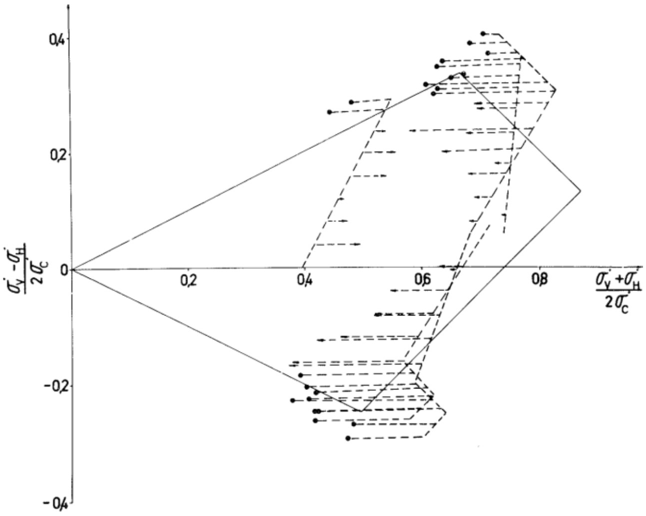

*Figure 2.10 Effective stress path for undrained creep tests. Black circles represents fail*ed tests *(Larsson, 1977).*

From the tests Larsson conducted he found a connection between the degree of mobilization and failure due to creep. Tertiary creep should with these findings occur if the degree of mobilization is higher than 80%. This valid for Lilla Mellösa clay but also tested for Drammen and Bäckebol clay.

3 Stress- strain relationships

The constitutive law establishes the relation between stresses and strains. It links the relation between the internal forces a material is subjected to with the deformation. The constitutive law is effected by many factors within the material like plasticity, viscosity, anisotropy etc. (Silva 2006). These relationships between stresses and strains are important when developing new and better finite element models. In soil mechanics the stiffness and strength are dependent on effective stresses, and therefore, all constitutive models should be expressed in effective stresses rather than total stresses. (Kullingsjö, 2007).

3.1.1 Elasticity

The simplest constitutive model is Hooke's law (1678) which says that the strain is proportional to the stress, see equation 3.1 below. This law describes an elastic behaviour of a material and can be described by a spring which is effected by a force. The spring will start to deform when the force is applied but the deformation will return to its initial state when the force is removed, which means that the behaviour of the material is the same in the loading and unloading phase.

$$\sigma = E\varepsilon \tag{3.1}$$

where σ is stress, ε is strain and E is the young's modulus of the material. The slope of the stress-strain relationship is the young's modulus, E, of the material. When a material is subjected to a deformation it will change form (Silva, 2006). This change in form is described by Poisson's ratio which describes the relation between the change in length and the change in width, see equation 3.2 below

$$\nu = \frac{\delta d}{d} / \frac{\delta l}{l} \tag{3.2}$$

where ν is Poission's ratio, d is width and l is the length. An isotropic material is a material which has the same rheological behaviour in all directions. An elastic isotropic material's behaviour can be described if Poissons' ratio, ν' and Young's modulus, E' are known. However, bulk modulus K' and shear modulus G' can be used instead. The relationship between Poisson's ratio, ν', Young's modulus, E', bulk K' and shear modulus, G' are shown in equation 3.3 and 3.4

$$K' = \frac{E'}{3(1-2\nu')} \tag{3.3}$$

$$G' = \frac{E'}{2(1+\nu')} \tag{3.4}$$

The bulk and shear modulus divides the elastic deformation into two separate parts, one volumetric, which is a change in size and one distortional, which is a change in shape at constant volume (Wood, 1990).

The stiffness matrix D for a material with full isotropic behaviour can be seen in the matrix 3.1 below (Kullingsjö, 2007).

Matrix 3.1 Stiffness matrix D for a fully isotropic elastic material.

$$
\begin{bmatrix} \delta\sigma'_{11} \\ \delta\sigma'_{22} \\ \delta\sigma'_{33} \\ \delta\sigma'_{23} \\ \delta\sigma'_{31} \\ \delta\sigma'_{12} \end{bmatrix} = \begin{bmatrix} A & B & B & & & \\ & A & B & & & \\ & & A & & & \\ & & & \frac{1}{2}(A-B) & & \\ & & & & \frac{1}{2}(A-B) & \\ & & & & & \frac{1}{2}(A-B) \end{bmatrix} \begin{bmatrix} \delta\varepsilon_{11} \\ \delta\varepsilon_{22} \\ \delta\varepsilon_{33} \\ \delta\varepsilon_{23} \\ \delta\varepsilon_{31} \\ \delta\varepsilon_{12} \end{bmatrix}
$$

The notation A and B in matrix 2.1 is described in equation 3.5 and 3.6 below.

$$A = \frac{E}{(1+v\prime)(1-2v\prime)}(1-v') \;=\; K + \frac{4}{3}G \tag{3.5}$$
$$B = \frac{E}{(1+v\prime)(1-2v\prime)}v' \;=\; K - \frac{2}{3}G \tag{3.6}$$

Where ν' is Poisson's ratio, E is young's modulus, K is bulk modulus and G is shear modulus. The elastic constants for soils can be deduced from triaxial compression tests.

3.1.2 Anisotropic elasticity

As discussed earlier, is it unrealistic to model soil as an isotropic material due to its formation. The soil has been affected by different stresses at different directions and is therefore more likely an anisotropic material. An anisotropic material has elastic constants that depend upon the orientation of the sample. These kinds of material need six independent stress components and six independent strain increments. These components can be expressed in a 6 x 6 matrix. For this material to be elastic the matrix need to be symmetric and due to that there is only a need of 21 independent parameters to describe elastic materials behaviour. However is it likely that many materials have a more limited anisotropy. If a material has an axis of symmetry in a way that the sample can be rotated around this axis without any change in the material it is called cross anisotropy. This is often the case for normal consolidated or lightly consolidated soils elastic properties, which depends upon the stress history of the soil and its deposition. A soil that has been deposit one-dimensionally with vertical deposition and in the same time subjected to equal horizontal stresses will be cross anisotropic. The behaviour of a cross anisotropic sample can be described by five independent elastic constants instead of 21 (Graham & Houlsby, 1983).

3.1.3 Elasto-plastic

Soils are more complex than the linear elastic behaviour described earlier, and improvements on describing the soil can be done by applying the theory of plasticity. The strains are then divided into two parts, one elastic ε^e and one plastic ε^p see equation 3.7. A plastic deformation is non-recoverable displacement due to a force and energy dissipation within a system (Silva, 2006). A simple model for elastic-plastic behaviour is shown in figure 3.2. (Potts & Zdravkovic, 1999)

$$\delta\varepsilon = \delta\varepsilon^e + \delta\varepsilon^p \tag{3.7}$$

where ε is total strain, ε^e is elastic strain and $\delta\varepsilon^p$ is plastic strains.

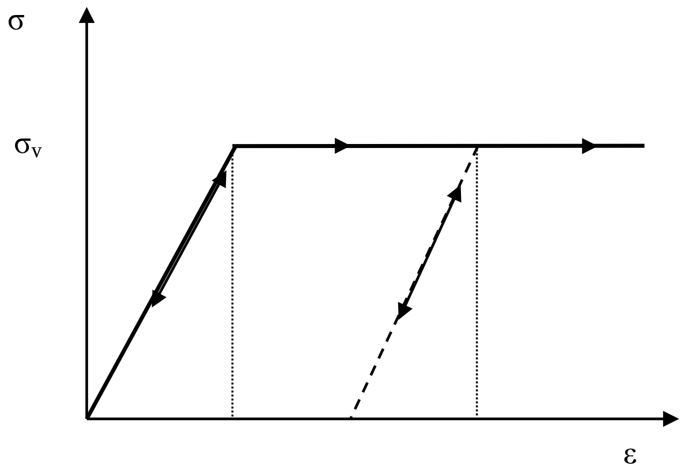

Figure 3.1 Elastic perfectly plastic material (Potts & Zdravkovic, 1999).

Two other stress strain models worth mentioning are the hardening and softening model which can be seen in figure 3.3. A material is behaving in a hardening manner if it the strength continues to increase after yielding. In the same way is a material considered softening if the strength is decreasing after yielding (Potts & Zdravkovic, 1999).

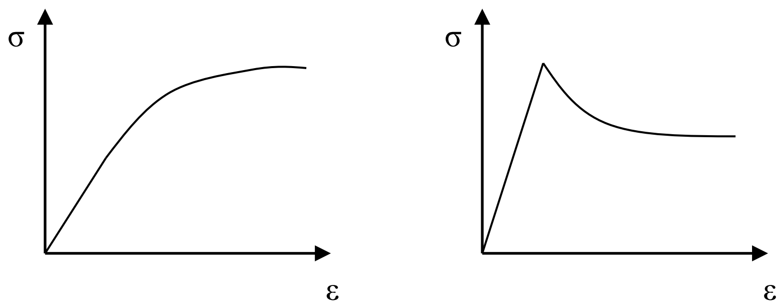

Figure 3.2 Picture on the right shows linear elastic strain hardening plastic material and the picture on the left linear elastic strain softening plastic material.

3.1.4 Elastic visco-plasticity

To be able to incorporate strain rate and visco plastic behaviour into constitutive models there is a need for a elastic visco-plastic theory. The strains are still the same as in the elasto-plastic model but it is assumed that all plastic strains that occur are time dependent, see equation 3.8 (Kullingsjö, 2007)

$$\delta\varepsilon = \delta\varepsilon^e + \delta\varepsilon^c \tag{3.8}$$

where ε is total strain, ε^e is elastic strain and $\delta\varepsilon^c$ is visco-plastic strains.

4 Excavations

There are mainly two kinds of excavations used today, the first one is gravity and freestanding walls and the second is embedded walls. Gravity walls stability is due to their weight and embedded walls stability is due to passive resistance of the soil over the part that is embedded in the soil and structural external support. When designing a retaining wall there are three main principles of limit states that have to be followed. The first is that an earth retaining structure may not collapse or suffer large damage, secondly it should not be any unacceptable deformations in relation to the wall and thirdly suffer from any minor damage that would increase excessive maintenance or reduce its anticipated lifetime.

In Sweden Eurocode 7 is followed when designing retaining structures. Eurocode 7 is separated into two limit states that must be considered. The first is Ultimate limit state which involves instability or collapse of the structure as a whole or failure in any components of the structure. The second limit state is the serviceability limit state which covers excessive deformations which leads to damage to the structure or loss of its function. This method is based on partial factors which are multiplied to actions and properties of the soil, the partial factors are either favourable or unfavourable depending on the effect it has on the structure. Before Eurocode 7 was introduced a global factor of safety was used. This factor of safety was based on the ratio between the resisting moment and the overturning moment of the wall. This method gave a high value which was enough to allow for uncertainties in the soil as well as in the analytical method.

Cantilever walls are often steel sheet pile walls that are used for lower heights of the retained soil. They are in general used as temporary but can be used as permanent in friction materials. The stability of the retained wall is due to passive resistance in the soil in front of the wall. Instability of a cantilever wall is mainly because of rotation or translation of the wall. The rotation is located around point a close to the lower end of the wall (Craig, 2004). In this thesis only temporary excavations retained by a cantilever sheet pile wall are investigated.

4.1 Behaviour of soft soil close to an excavation

The behaviour of soft soil is dependent on its stress history. The stress state of a specific soil sample is a result of the deposition of the soil, erosion in the area where it was deposited and activities nearby such as excavations and buildings (Kullingsjö, 2007). A usual way of describing the soils behaviour and the concept is by using stress paths which will be described in the following chapter.

4.1.1 Stress paths

Mohr’s circles are a graphical representation of the stress state of a point in a specimen. The abscissa of the circle describes the normal stress σ_n and the shear stress τ_n is described by the ordinate.

During a loading process it is possible to describe the evolution of Mohr’s circles as a stress path in terms of s’ and t where s’ is the stress coordinate from the centre of Mohr’s circle and t is the radius of it. The abscissa of Mohr’s circle is presented as a single point and if the stress state varies the point move and a stress path is shown. The equations for the effective s' and t' can be seen in equation 4.1 and 4.2

$$s' = \frac{1}{2}(\sigma'_1 + \sigma'_3) \tag{4.1}$$

$$t' = \frac{1}{2}(\sigma'_1 - \sigma'_3) \tag{4.2}$$

where σ_1 is the major principle stress and σ_3 is the minor. Different type of constructions gives different stress changes to the soil. These changes can be visualised in s'-t space. Point A in figure 4.1 shows the initial stress state of the soil before any construction. The line AB and AB' describes the change in total and effective stress due to the construction (Bardet, 1997).

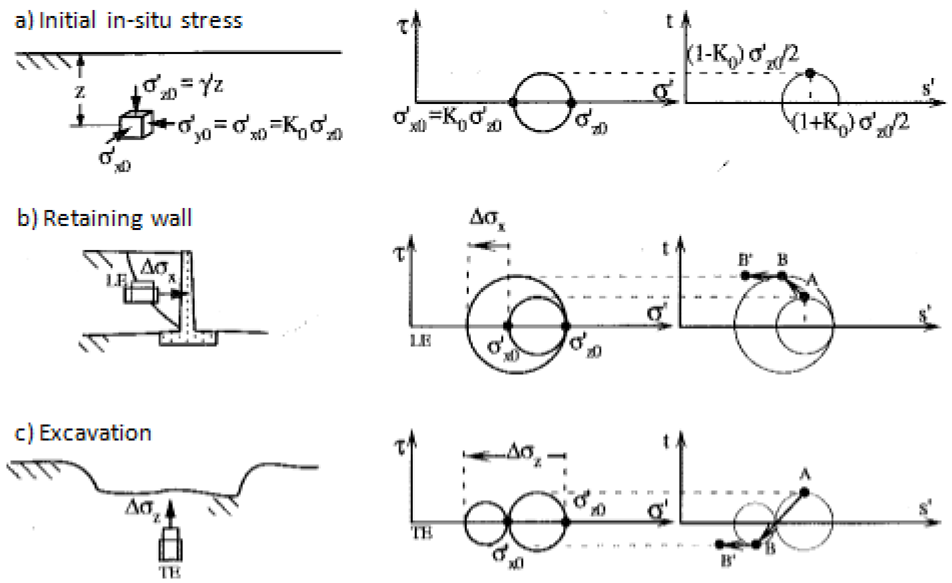

Figure 4.1 Figure a show in-situ stresses for a soil specimen and figure b, c shows stress changes resulting from a retaining wall and an excavation. (Bardet, 1997)

The soil located on the retained side of an excavation will lose lateral support during the excavation and the horizontal stress will decrease, see figure 4.1b, while the soil beneath the excavation will be unloaded and there will be a decrease in vertical stress, see figure 4.1c.

Depending on where the soil is compared to the stress change different shear strengths will show, see Figure 4.2. The shear strengths below the excavation are lower than the shear strength next to the retained wall (Kullingsjö, 2007).

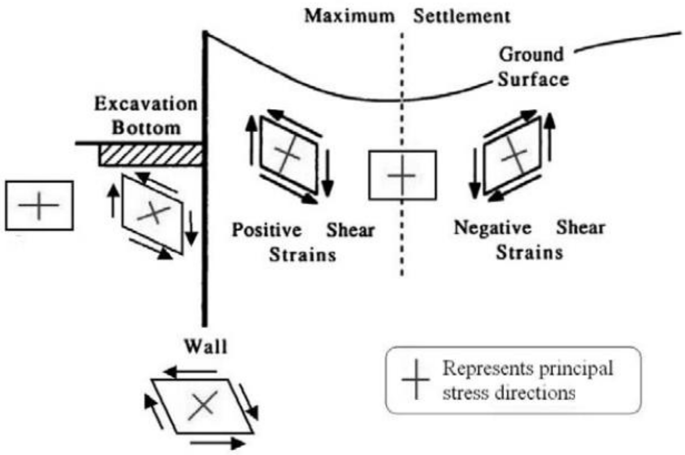

Figure 4.2 Stresses and their directions at different points at an excavation (Kullingsjö, 2007).

4.1.2 Stress paths at an excavation

The behaviour of a soft soil is primarily governed by the effective stresses in the soil which are dependent from the drainage situation. The critical case for an excavation is when one of several failure mechanisms in the retaining structure occurs. Example of failure mechanisms that can occur to an retaining structure are overturn of the structure, sliding of the structure, bearing capacity, bending of the wall or some stability problems of the soil around the excavation. When designing a retaining structure both the long term and the short term safeties are important factors to control. A retaining structure is mostly associated with unloading and decreased level of stresses. It is therefore usual to carry out long term analysis in terms of effective stresses and strength parameters because this usually is the critical case for the structure (Kempfert & Gebreselassie, 2006).

There are different drainage situations around an excavation, and due to this there will be different changes in stress. These different drainage situations can be separated into three categories. The first one is a drained situation, where no excessive pore pressure is generated. The second is a undrained situation with constrained conditions there no volume change is possible, this will generate excessive pore pressure in the soil. The last situation is partly drained, in this situation will excessive pore pressure develop but dissipate again over time. Excavations are theoretically placed in the third category but the time of the drainage differs depending on the hydraulic conductivity in the soil. A temporary excavation is placed in the second category and is therefore considered to be undrained until its final stage. Any drainage that occurs under a temporary excavation is due to time-delayed deformations. To be able to observe this behaviour is the consolidation of the soil necessary to be taken into account (Kullingsjö, 2007).

In figure 4.3 is the effective stress path A'B' corresponding to an undrained loading and B'C' corresponds to swelling and a decrease in mean normal effective stress. The pore pressure u_i which is immediately after construction is smaller than the pore pressure u_c which is final steady state pore pressure. This indicates an excessive pore pressure in the beginning which is negative. The total stresses are shown in AB and remains the same even when the pore pressure rises. The retaining structure will fail if any stress point reaches the failure line. If B' reaches the failure line is failure occurring during the undrained excavation and if C' reaches the line the structure fails some time after the completed construction. The factor of safety decreases with drainage as demonstrated in the figure.

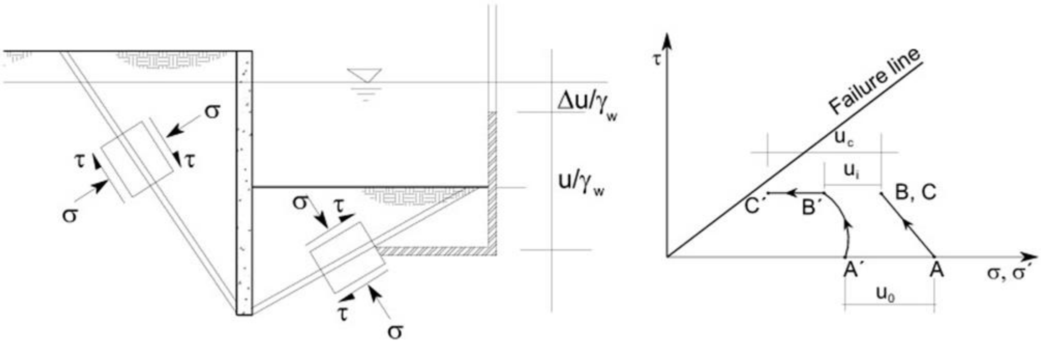

Figure 4.3 Change of stress and pore pressure at an excavation shown in effective and total stress paths (Kempfert & Gebreselassie, 2006).

5 Laboratory test

As discussed earlier, soil is exposed to different types of loading situations by different constructions. During an excavation vertical stresses decrease, while when an embankment is constructed the vertical stresses increase instead. To be able to determine the response of the soil is it important to determine the stress strain response and shear strength of a soil by subjecting the soil to a similar situation as the soil will be subjected to during and after construction. This is usually done in the laboratory. This chapter describes two different laboratory tests that are necessary for this thesis work. The laboratory tests that will be used in this thesis are oedometer test and triaxial tests.

5.1 Oedometer test

The oedometer test is one of the most common tests in Sweden. It gives a necessary data for consolidation calculations and a basic understanding of the soil behaviour. There are two different kind of oedometer tests used today. The first one has an incremental loading which is the classic test and the second one has a constant rate of strain CRS during the whole test. (Havel, 2004)

The soil sample in a standard oedometer test has a height of 20 mm and a diameter of 50 mm and is placed into a cylindrical oedometer ring. There is a porous material both below and on top of the test where drainage can occur. The load is applied from the top of the test with either a constant rate of strain or as an incremental load. The soil sample is covered in water during the test sequence (Larsson, 2008). The test equipment can be seen in the schematic picture in figure 5.1.

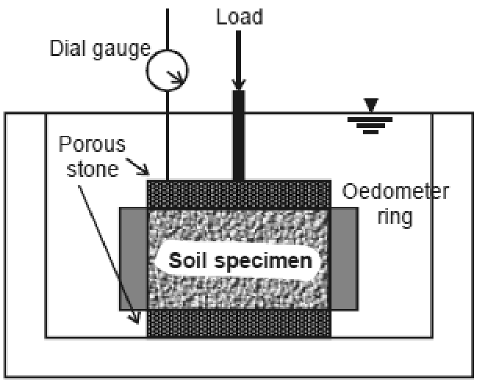

Fig 5.1 Schematic figure over an oedometer apparatus (Havel, 2004)

The result from the test is often displayed in a curve with void ratio e and log σ*'*, but this kind of evaluation is not common in Sweden where the vertical effective stress is plotted against the compression instead.

The incremental loading test is necessary if creep is relevant for the project or the problem that is investigated given it is possible to derive creep properties and compression index (Havel, 2004). In an incremental loading test is the load doubled every 24 hour (Larsson, 2008). A normal standard procedure has eight incremental steps with start on 10 kPa. With the result from this test is it possible to derive the preconsolidation pressure of the soil, the compression modulus and the secondary compression index (Sällfors & Andréasson, 1985).

In a constant rate of strain test is the vertical load applied in a constant speed, the standard speed used in Sweden is 0.72 %/hour. During the test are pore water and the applied load measured. The result from this test gives the compression modulus, the permeability of the soil, and the preconsolidation pressure (Sällfors & Andréasson, 1985).) The preconsolidation pressure need to be corrected to account for rate effects.

5.2 Triaxial test

Triaxial test is also widely used in soil mechanics. This kind of test is mainly used for determination of shear strength parameters (Havel, 2004). A standard soil sample has a height of 100 mm and a diameter of 50 mm. The specimen is placed inside a membrane on a bottom plate that is either porous or solid. The specimen is sealed with a top cap in the same material as the bottom. The chamber around the soil specimen is filled with water where the soil can be subjected to an even pressure against the membrane. An axial load can be applied vertically on the top plate and the drainage condition for the test is controlled by a tap. The test can either be controlled by stress or strain (Havel, 2004). A principal sketch over the triaxial apparatus can be seen in figure 4.2.

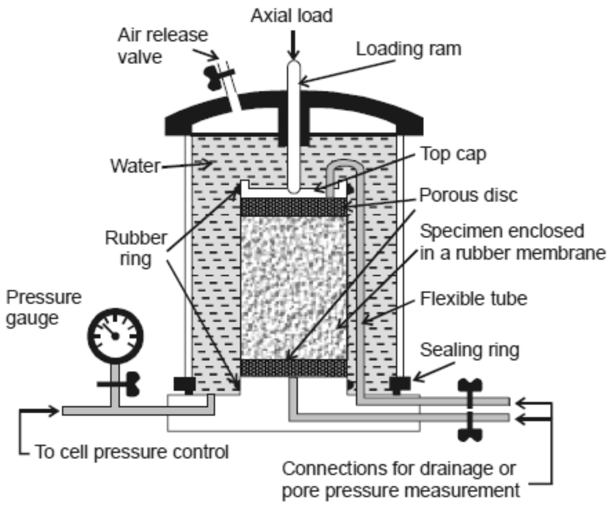

Figure 5.2 Schematic figure over a triaxial test apparatus (Havel, 2004).

There are two kinds of triaxial tests, compression and extension, in Sweden called active and passive. These tests can either be conducted drained or undrained. A drained test is conducted with the valves open and no pore pressure will develop and therefore are the effective and total stresses the same. In an undrained test are the valves closed and there is a pore pressure in the specimen which generates different effective and total stresses (Bardet, 1997). In a compression test is the sample being compressed to failure with an increased load and in a extension test is the loading decreased until the soil reaches failure in extension. The soil sample is usually consolidated before the start of the test. In the consolidation phase is the soil sample subjected to stresses that to correspond to the soils in situ conditions. All drained tests are always consolidated (Infrastruktur, 2005). The consolidation phase is either isotropic or a K_0-consolidation. K_0 is the lateral earth pressure at rest. (Bardet, 1997). During an isotropic test is K_0 = 1and it is assumed that the vertical stress is equal to the horizontal stress. An undrained, K_0-consolidated compression test is noted CK_0UC and a undrained K_0-consolidated extension test is noted CK_0UE.

Figure 5.3 shows consolidation of an isotropic and one K_0 loading of test.

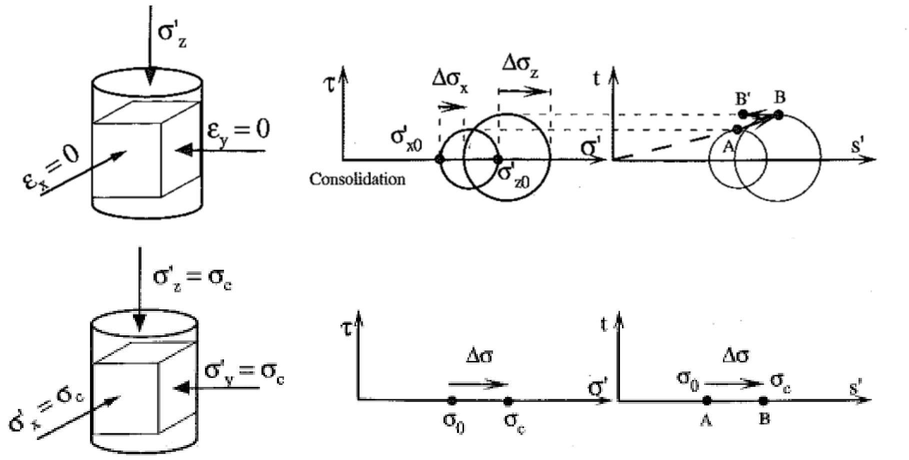

Figure 5.3 The figure at the bottom shows the stress path for an isotropic loading and the figure at the top shows a stress path for K0 consolidation (Bardet, 1997).

Figure 5.4 shows the stress path for different triaxial tests.

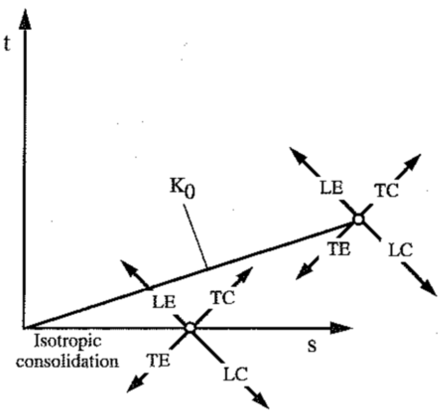

Figure 5.4 Stress paths in s-t space during K0 and isotropic consolidation for TC- triaxial compression, TE triaxial extension, LC lateral compression and LE lateral extension (Bardet, 1997).

The parameters that can be derived from triaxial tests are the soils shear strength, friction angle, cohesion, dilatancy angle with others (Havel, 2004).

6 Models for simulating behaviour of soft soils

6.1 Critical state concept of soils

The critical state concept of soils was developed by Schoefield and Wroth in 1958. Their idea was that soils and granular materials would come to a critical state when they are continuously distorted until they flow as a frictional fluid and are perfectly plastic without any volume change. This critical state could be described by equation 6.1 and 6.2.

$$q = Mp \tag{6.1}$$

$$\Gamma = v + \lambda \ln p \tag{6.2}$$

where q is the deviator stress which is $\sigma_{1-}\ \sigma_{3,}$ M is a frictional constant, p is the mean stress defined as $(\sigma_{1+}\ \sigma_{2+}\ \sigma_{3)}/3$, v is specific volume, Γ is the location of critical state line in compression plane and λ is the normal compression line in v:lnp space.

The first of the two equations defines the magnitude of deviator stress q that is needed for the soil to keep flowing continuously as a product of a frictional constant M. The second equation describes how the specific volume v, will decrease as the effective pressure increases as a semi logarithm fashion (Schoefield & Wroth, 1968).

If the soil is more compact than the critical state it is called to be on the dry side, and during deformation it will then expand. If the soil state lies right of the critical line it is called to be in wet state, then the pore pressure is increasing with the total stress and will later be dissipated from the soil if possible. With this concept is it possible to predict the total change from the initial state to an ultimate critical state (Schoefield & Wroth, 1968).

With the critical state is it easier to model in a comprehensive manner the behaviour of a soil specimen compared to a perfectly plastic model such as Mohr Coulomb. A more realistic elastic-plastic model needs four different parameters to work. The four parameters are elastic properties of the soil, a yield surface, a plastic potential and a hardening rule.

The elastic properties of a soil have already been discussed. A yield surface represents a boundary in the stress space where the elastic deformations change to elastic plastic deformations. Any change inside the yield surface is elastic and completely recoverable. The position and size of yield surface is dependent on the preconsolidation pressure of the soil. When the stress state of a soil reaches yield surface the deformations becomes plastic and irrecoverable. With this increased stress state, which is higher than the preconsolidation pressure, the yield locus expand.

This expansion of the yield locus can be expressed as a volume change in the compression plane v:lnp'. This plane consists of a set of lines, one normal compression line (ncl), see equation 6.3 and either one or more unloading reloading lines (url), see equation 6.4.

$$v = v_\lambda - \lambda \ln p' \tag{6.3}$$

$$v = v_\kappa - \kappa \ln p' \tag{6.4}$$

Where λ and κ are the slope of the normal- and unloading/reloading - lines in the compression plane v:ln p´ and v_λ and v_κ are intercepts on the lines at p´ = 1, p' is the effective mean stress and v is the specific volume.

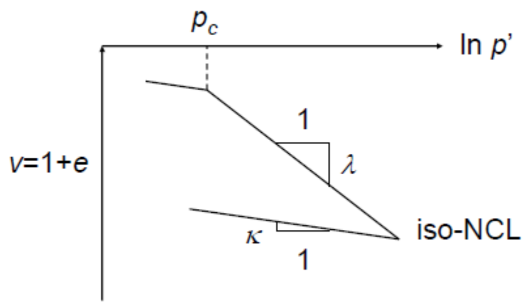

Figure 6.2 Normal compression line and unloading reloading compression line in the compression plane (Potts & Zdravkovic, 1999).

Any volume changes that occur along the normal compression line will be mainly irrecoverable plastic deformations, while the volume change along unloading and reloading line is elastic and recoverable (Potts & Zdravkovic, 1999). The plastic strains that affect the yield locus are a combination of plastic shear strains, $\delta\varepsilon_q^p$, and plastic volumetric strains, $\delta\varepsilon_v^p$. As mentioned earlier, the volumetric strains are dependent on the mean effective stress p' and the shear strains are dependent on the deviator stress q. The plastic strains can with that information be drawn as a vector S, see figure 6.3 and orthogonal to them can a small line be drawn. (Wood, 1990).

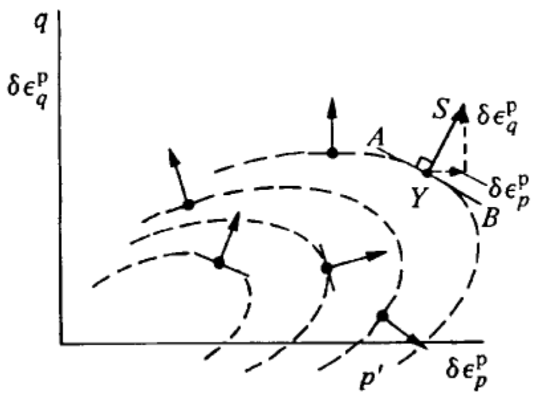

Figure 6.3 Plastic strains and their direction (Wood, 1990).

With several yield points, and their strain vectors it is possible to link the orthogonal lines into a plastic potential. The plastic potentials can either be associated or non-associated with the yield curves. If the plastic potentials are associated it means that they have the same shape as the yield curve (Wood, 1990). The hardening law controls the plastic strains and links the strains with the increased yield surface (Kullingsjö, 2007).

6.2 Hardening soil model

The hardening soil model was developed by Schantz 1998 and is a hyperbolic model which has a relationship between the vertical strain ε and the deviatoric stress q. The model is formulated as a double stiffness model for elasticity and strain hardening. It also includes soil dilatancy and has a yield cap. The yield surface is not fixed in the Hardening Soil model and can expand due to plastic straining in contrast to Mohr-Coulomb which is a perfectly plastic model. The model separates between two main types of hardening, shear hardening and volumetric hardening. The Hardening Soil model has three different stress dependent stiffness parameters, primary shear stiffness E_{50}, primary compression stiffness E_{oed} and unloading reloading stiffness E_{ur}. The amount of stress dependency is decided by the power m, which is set to 1 for soft clays to enable semi logarithmic stress dependency. The power m describes the curvature in the relationship between q and ε and means that the stiffness in the soil increases with depth (Schanz et al.1999). The limiting states of stress is described with Mohr-Coulombs failure criteria with the friction angle φ', apparent cohesion c' and dilatancy ψ.

The basic formulation for the hardening soil model is based on Duncan and Chang's model from 1970. They formulated a hyperbolic stress strain relationship in a model for triaxial loading with Mohr Coulombs failure criteria, see equation 6.5 - 6.7.

$$q < q_f \qquad : -\varepsilon_1 = \frac{1}{\mathrm{E_i}} \frac{q}{1-q/q_a} \tag{6.5}$$

$$q_f = \frac{2sin\varphi}{1-sin\varphi}(\sigma'_3 + c\cot\varphi) \tag{6.6}$$

$$q_a = \frac{q_f}{R_f} > q_f \tag{6.7}$$

Where ε_1 is the vertical strain, q is the deviatoric stress in primary loading, q_a is an asymptotic value for shear strength, E_i is a stiffness for initial state and related to $E_{50,}$ which is stiffness modulus for primary loading, by equation 6.9, q_f is an ultimate deviatoric stress and Rf is a failure ratio which has a default value at 0.9. This stress strain relationship can be seen in figure 6.4. When failure value of q_f is reached there are no more deviatoric strains.

The input values $E_{50,}$ E_{oed} and E_{ur} for the hardening soil model are reference values that are based on a reference stress, p^{ref} which is usually set to 100 kPa. E_{oed} is the plastic cap hardening secant modulus for 1D compression, E_{50} is the plastic cone hardening secant modulus and E_{ur} is the elastic unloading and reloading modulus.

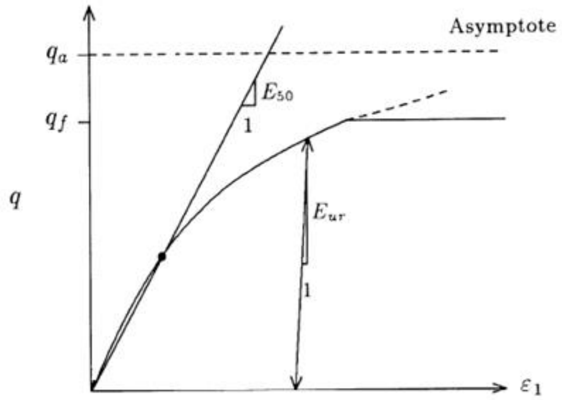

Figure 6.4 Stress strain relationship for a standard drained triaxial test in primary loading. (Schanz et al.1999)

There are two yield functions for the hardening soil model, the first one is for shear hardening, which is the cone, and the second one is for volumetric hardening, which is the cap, see figure 6.5.

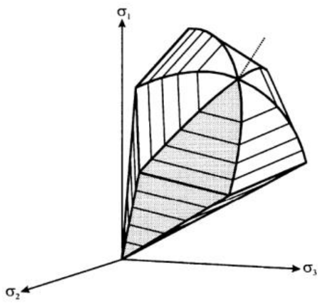

Figure 6.5 The yield surface for the hardening soil model in principal stress space (Schanz et al.1999).

The cones yield function f^s which controls the shear hardening is expressed as

$$f^s = \frac{2}{E_i}\frac{q}{1-q/q_a} - \frac{2q}{E_{ur}} - \gamma^p \tag{6.8}$$

$$E_i = 2E_{50}/(2-R_f) \tag{6.9}$$

where γ^p is a plastic shear strain parameter describing where the opening of the cone are and E_i is the initial stiffness E_{ur} is the stiffness for unloading reloading, E_{50} is stiffness modulus for primary loading, q deviator stress, q_a is an asymptotic value for shear strength and Rf is a failure ratio. With increasing plastic shear strains the cone will move closer to Mohr Coulombs failure line until failure is reached. In triaxial shearing where $\sigma_2 = \sigma_3$ is it assumed that the plastic volumetric strain is insignificant against the axial strain. And therefore is

$$\gamma^p = 2\varepsilon_1^p - \varepsilon_v^p \approx 2\varepsilon_1^p \tag{6.10}$$

where ε_1^p is vertical plastic strains and ε_v^p is plastic volumetric strains, which gives the expression for plastic axial strain when f = 0 as

$$\varepsilon_1^p = \frac{1}{E_i}\frac{q}{1-q/q_a} - \frac{2q}{E_{ur}} \tag{6.11}$$

where q_a is an asymptotic value for shear strength, E_i is a stiffness for initial state, q is the deviatoric stress and E_{ur} the unloading/reloading stiffness. The elastic strains that appear both during the elastic and elasto-plastic stage can be expressed as

$$\varepsilon_1^e = \frac{q}{E_{ur}} \tag{6.12}$$

where q is the deviatoric stress and E_{ur} is the unloading/reloading stiffness. The flow rule for the hardening soil model is expressed in terms of plastic volumetric strains. The flow rule is linear and expressed as

$$\dot{\varepsilon}_v^p = sin\psi_m\dot{\gamma}_p \tag{6.13}$$

where ψ_m is the mobilised dilatancy angle, defined as the ratio between the plastic volumetric strain and deviatoric plastic shear strain and $\dot{\gamma}_p$ is the hardening parameter (Schanz et al.1999).

The cap yield function $f^{\,c}$ controls the volumetric hardening and without this cap that closes the p-axis it would not be possible to have two independent moduli, E_{50} and E_{oed}. The cap yield surface is controlled by the oedometer modulus and the earlier mentioned cone is controlled by the triaxial modulus. The yield surface of the cap is expressed as

$$f^c \ = \frac{\tilde{q}^2}{\alpha^2} - /(p' + c'cot\varphi')^2 - (p_p + c'cot\varphi')^2 \tag{6.14}$$

$$\tilde{q} = \sigma'_1 + (\delta - 1)\sigma'_2 - \varphi\sigma'_3 \tag{6.15}$$

$$\delta = \frac{3+sin\varphi}{3-sin\varphi} \tag{6.16}$$

where p_p is the isotropic preconsolidation pressure that decides the position of the cap and α is related to K_0^{nc}. σ'_1 is the major effective principal stress, σ'_2 is the intermediate and σ'_3 is the minor. c' is the apparent cohesion, φ' mobilized friction angle. The default value for $K_0^{nc} = 1\text{-}sin\varphi_p$ (Schanz et al.1999).

The hardening law for the yield cap is expressed in equation 6.28

$$\varepsilon_v^{pc} = \frac{\beta}{1-m}\left(\frac{p_p}{p^{ref}}\right)^{1-m} \tag{6.17}$$

where β is related to E_{oed}^{ref}. p^{ref} is a reference pressure with default value on 100 kPa. The values α and β can therefore be calculated by the means of E_{oed}^{ref} and K_0^{nc}. The yield cap is formed as an ellipse and starts at p_p on the p axis and at αp on the q axis, see figure 6.6 (Plaxis, Version 1).

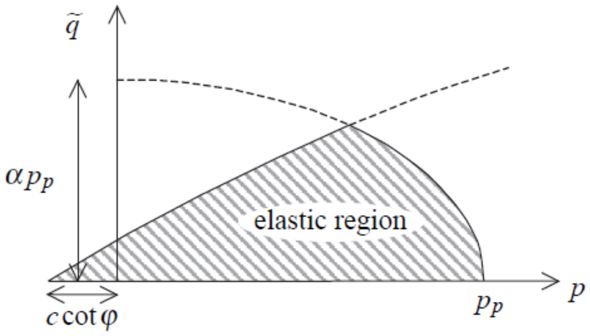

Figure 6.6 Yield surface of the hardening soil model in p-q plane (Plaxis, Version 1).

The input values for the hardening soil model can be seen in table 6.1.

Table 6.1 Input parameters for the hardening soil model (Plaxis, Version 1).

Failure parameters Mohr-Coulomb	
c'	Effective cohesion (kN/m^2)
Φ'	Effective angle of internal friction (°)
Ψ'	Angle of dilatancy (°)
Parameters for soil stiffness in terms of effective stresses	
E_{50}^{ref}	Secant stiffness in standard drained triaxial test (kN/m^2)
E_{oed}^{ref}	Tangent stiffness for primary oedometer loading (kN/m^2)
E_{ur}^{ref}	Unloading/Reloading stiffness (kN/m^2)
m	Power for stress level dependency of stiffness (-)
Advanced parameters	
v_{ur}	Poisson's ratio for unloading/reloading
p^{ref}	Reference stress for stiffnesses
K_0^{nc}	K_0-value for normal consolidation
Rf	Failure ratio qf/qa

6.3 Creep-SCLAY1S

As mentioned in the introduction, many researchers have focused on developing key features of soils behaviour, which has generated a lot of different models incrementally over the last decade. Creep-SCLAY1S was presented by Sivasithamapam et al. (2012) and is the latest of these models that accounts for all three key issues; anisotropy, destructuration and creep. Creep-SCLAY1S is implemented as a user-defined model and is hence not a standard PLAXIS model. Creep-SCLAY1S is based on ACM anisotropic creep model by Leoni et al. (2008) and S-CLAY1S by Karstunen et al. (2005). In Creep-SCLAY1S the creep is formulated using a visco-plastic multiplier (Grimstad et al. 2010)instead of the formulation from ACM which was based on the assumption of contours of volumetric creep strain rates. The main difference between these two formulations is that critical state condition could not be met or exceeded in the formulation of contours of volumetric creep strain, but also that the ACM, exaggerated the results of creep in many situations due to its unrealistic model formulation.

One concern about the ACM was that the model could not predict any swelling on the dry side, see fig 6.7. This is due to that the stress is not allowed to cross Mohr Coulomb failure line. Moreover, it cannot perform satisfactory results of strain rate in undrained conditions for normally consolidated clays. With Creep-SCLAY1S is it possible to cross the failure line and model swelling at the dry side, figure 6.7 shows a comparison between ACM and Creep-SCLAY 1S where it is possible to see that the later one can predict results on the dry side (Sivasithamparam et al. 2013).

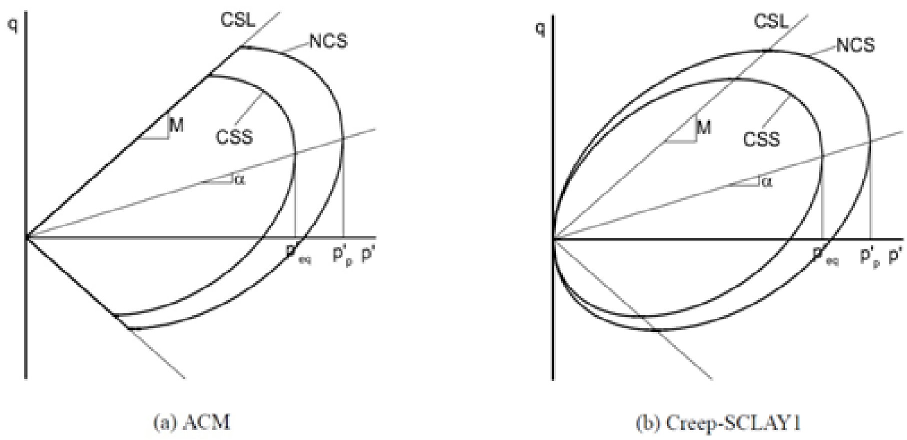

Figure 6.7 Comparison of yield surface for ACM and Creep-SCLAY1S (Sivasithamparam, Karstunen, Brinkgreve, & Bonnier, 2013)

The plastic multiplier for Creep-SCLAY1S is formulated in equation 6.18.

$$\dot{\Lambda} = \frac{\mu^*}{\tau}\left(\frac{p'_{eq}}{p'_p}\right)^{\beta}\left(\frac{M^2-\alpha^2}{M^2-\eta^2}\right) \qquad (6.18)$$

Where β is defined in equation 6.19, η is the ratio of q over p in K_0^{NC} loading, p'_{eq} is equivalent mean stress, p'_p is preconsolidation pressure, α is the rotation of the yield surface, with initial value corresponding to in K_0^{NC} loading, M is the critical state line and μ^* is the modified creep index defined in equation 6.20 below

$$\beta = \frac{\lambda^* - \kappa^*}{\mu^*} \tag{6.19}$$

$$\mu^* = \frac{C_\alpha}{ln10(1+e_{0)}} \tag{6.20}$$

where e_0 is the initial void ratio and C_α is the secondary compression index. To limit the creep strains is another term introduced to the plastic multiplier which is based on void ratio. When the void ratio reaches e_{min} the creep will stop see equation 6.21 for the addition to equation 6.18.

$$\dot{\Lambda} = \frac{\mu^*}{\tau}\left(\frac{p'_{eq}}{p'_p}\right)^\beta \left(\frac{M^2-\alpha^2}{M^2-\eta^2}\right)\left(\frac{e-e_{min}}{e_0-e_{min}}\right) \tag{6.21}$$

Where the new parameters are current void ratio e, initial void ratio e_0 and minimum void ratio e_{min}.

The associated flow rule is formulated in equation 6.22

$$\dot{\varepsilon}_{ij}^c = \dot{\Lambda} \frac{\partial p'_{eq}}{\partial \sigma'_{ij}} \tag{6.22}$$

where Λ is the plastic multiplier. And the increment of plastic strains are formulated as

$$\Delta\varepsilon_{ij}^c = \Delta t \dot{\Lambda} \frac{\partial p'_{eq}}{\partial \sigma'_{ij}} \tag{6.23}$$

where t is time.

Creep-SCLAY1S has three hardening laws. The first hardening law is from the model S-CLAY1 by Karstunen et al. (2005). This law relates to the change in size in the intrinsic yield surface, which only is related to plastic volumetric strains.

$$\Delta p'_{mi} = \frac{p'_{mi}}{\lambda_i^* - \kappa^*}\Delta\varepsilon_v^p \tag{6.24}$$

Where λ_i^* is the intrinsic modified compression index for reconstituted soil, $\kappa^*$is the modified swelling index and p'_{mi} is a state variable defined in equation 6.25 and ε_v^p is volumetric plastic strains.

$$p'_m = (1-\chi)p'_{mi} \tag{6.25}$$

where χ is destructuration and p'_m is related to the size of the natural yield surface. If the destructuration parameter χ is chosen to zero the model neglects destructuration and the first hardening law is reduced to the same as in Modified Cam Clay, see equation 6.26

$$\Delta p'_m = \frac{p'_m}{\lambda^* - \kappa^*}\Delta\varepsilon_v^p \tag{6.26}$$

See explanation for the terms in the equation above.

The second hardening law is from the model by Wheeler et al. (2003) and is a rotational hardening law which describes how the yield surface orientates with the plastic straining.

$$\Delta\alpha_d = \omega\left(\left[\frac{3\sigma'_d}{4p'} - \alpha_d\right] \ \langle\Delta\varepsilon_v^p\rangle + \omega_d\left[\frac{\sigma'_d}{3p'} - \alpha_d\right]\Delta\varepsilon_d^p\right) \tag{6.27}$$

Where ω and ω_d are soil constants. The first one governs the rate at which α_d changes with plastic straining and the second one describes the relative effectiveness of plastic volumetric strain and plastic shear strain in rotating the yield curve. The Macaulay brackets governs over the $\Delta\varepsilon_v^p$ term and

$$\langle\Delta\varepsilon_v^p\rangle = \ \Delta\varepsilon_v^p \, for \, \Delta\varepsilon_v^p > 0 \ \ and \ \ \langle\Delta\varepsilon_v^p\rangle = \ 0 \tag{6.28}$$

$$for \ = \ \ \Delta\varepsilon_v^p < 0$$

The third and last law is also from Karstunen et al. (2005) and this law describes the degradation of bonding with plastic straining. The formulation is described in equation 6.29

$$\Delta\chi = -\xi\chi\left[\left|\Delta\varepsilon_v^p\right| + \xi_d\left|\Delta\varepsilon_v^p\right|\right] \tag{6.29}$$

where ξ and ξ_d are soil constants which controls the degradation and the rate of it.

The critical state line M has in Creep-SCLAY1S been made a function of Lode's angle. Lodes angle is incorporated a smooth failure yield surface as an option to Mohr Coulomb failure surface. The advantage for the new failure surface is that sharp corners are avoided. If the failure line for compression M_c is chosen to the same as the failure line for extension M_e is the model adopting Drucker-Prager failure criterion (Sivasithamparam et al. 2012). Table 6.2 presents the parameters for the model Creep-SCLAY1S.

Table 6.2 Parameters of Creep-SCLAY1S (Sivasithamparam N. , 2012)

Isotropic parameters MCC	
ν'	Poisson's ratio
M	Stress ratio at critical state in triaxial compression
λ_i^*	Slope of post yield compression line in e-ln p' space for reconstituted sample
λ^*	Slope of post yield compression line in e-ln p' space
κ^*	Slope of swelling/recompression line in e-ln p' space
Anisotropic parameters S-CLAY1	
ω	Absolute effectiveness of rotational hardening
ω_d	Relative effectiveness of rotational hardening
Destructuration parameters S-CLAY1S	
ξ	Absolute rate of destructuration
ξd	Relative rate of destructuration
Viscous parameters Creep-SCLAY1S	
μ^*	Modified creep index
τ	Reference time
Initial state parameters	
α_0	Initial inclination of the yield surface
χ_0	Initial bonding
POP	Pre-overburden pressure
OCR	Over-consolidation ratio
e_0	Initial void ratio

7 Input parameters for the models

In the next section three different cases will be modelled in two different models, the Hardening Soil model and Creep-SCLAY1S. Before these cases are presented parameters from laboratory tests will be adjusted for the models. The method for retrieving input parameters is described in this Section.

All cases are applied on the same area with the parameters presented below. The investigated area consists of a 70 m deep layer of clay with bedrock beneath. The water content in the clay is presented in Appendix A.1 and the clay profile is divided into four sub layers according to the water content. The sub layers are 0-7 m, 8-15 m, 16-30 m, 31-70m.

7.1 Parameters for the Hardening soil model

The parameters for the hardening soil model are derived from CRS oedometer test and undrained confined triaxial tests. The ideal triaxial test for this model is a drained triaxial test which is not feasible in clay because it is time consuming test and the deformation are often so large that the equipment runs out of travel. If a drained triaxial test is performed, creep might affect the results making them hard to analyse. There are no drained triaxial tests available and some values will be modified from an undrained triaxial test to a drained one to fit the model.

Values for the for the primary compression stiffness reference value E_{oed}^{ref} are calculated from equation 7.1. The soil in the area is clay and the apparent cohesion, c' is therefore assumed to be 0 and the power for stress level dependency of stiffness, m is assumed to be 1. Values of E_{oed} are evaluated from the constrained modulus between vertical preconsolidation pressure and σ'_L, M_L which is derived from CRS tests. The preconsolidation pressure, σ'_p is used for the major principle stress, σ'_1 to enable the use of the modulus M_L instead of E_{oed}. p^{ref} is chosen to the default value in PLAXIS at 100kPa. φ is the friction angle of the soil of 35°

$$E_{oed} = E_{oed}^{ref}\left(\frac{\sigma'_1 + c\cot\varphi}{p^{ref} + c\cot\varphi}\right)^m \tag{7.1}$$

With these values are E_{oed}^{ref} calculated and presented over depth in Figure 7.3.

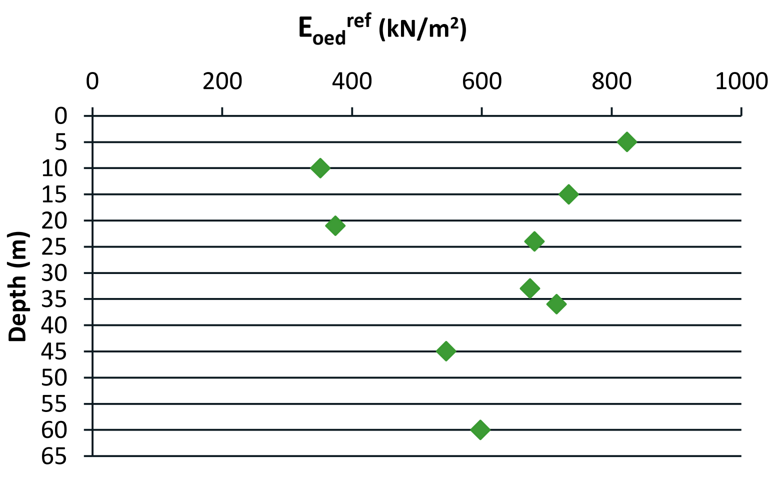

Figure 7.3 Values of E_{oed}^{ref} over depth.

The elastic unloading reloading stiffness E_{ur}^{ref} is calculated from a CRS test as well. The ideal test for this parameter is from a drained triaxial test and because no such tests has been performed has this value been modified to fit the model. The value that has been used from the CRS test is the constrained modulus below the effective vertical preconsolidation pressure been used, M_0 and $E_{oed,ur}$ has been calculated according to equation 7.2.

$$E_{oed,ur} = \frac{E_{ur}(1-v_{ur})}{(1-2v_{ur})(1+v_{ur})} \tag{7.2}$$

M_0 has been used instead of $E_{oed,ur}$ and unloading/reloading Poisson's ratio, v_{ur} is chosen to a low value around 0.2. Values of modulus M_0 evaluated from CRS test are lower than the field value due to sample disturbance and it is a common practice to multiply this modulus retrieved from CRS test with a factor of 3-5 (Olsson, 2010). The result of the elastic unloading tangent modulus, E_{ur} is used in equation 7.3. The same assumptions as mentioned before is used for c'=0 and m = 1. The preconsolidation pressure, σ'_p are used for the minor effective stress, σ'_3, φ is the friction angle of the soil of 35°.

$$E_{ur} = E_{ur}^{ref}\left(\frac{\sigma'_3 + c\cot\varphi}{p^{ref} + c\cot\varphi}\right)^m \tag{7.3}$$

The results for E_{ur}^{ref} over depth can be seen in Figure 7.4.

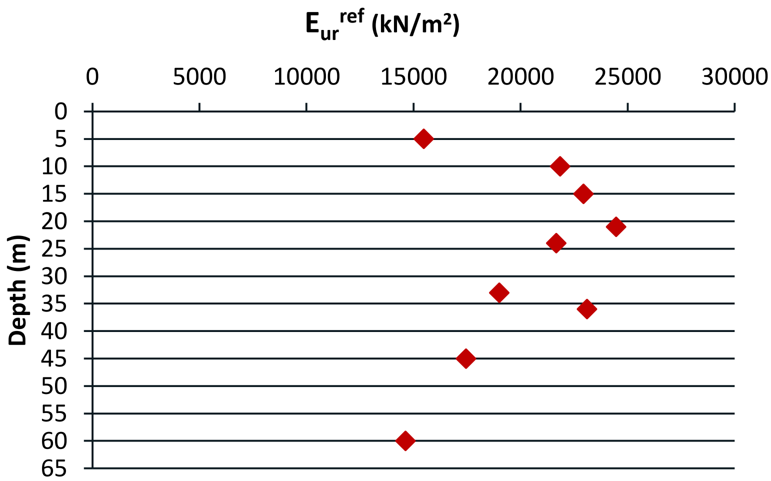

Figure 7.4 Values of E_{ur}^{ref} over Depth.

The last parameter that needs to be derived for the Hardening Soil model is the reference value for the stiffness modulus for primary loading, E_{50}^{ref}. This value is ideally collected from a drained triaxial test and because none of these tests are available are values from undrained triaxial tests modified to fit the model. Different methods of modifying this value are available, although no tests have been done on Scandinavian clays. However, Lambe and Whitmans (1969) method for this should be the best because they performed tests on North American clay which should be comparable to Scandinavian clays. Their solution was to multiply the value of E_{50} with a factor f see equation 7.4 where the value of f is in the interval of $0.25 < f < 0.35$.

$$E_{50} = f \cdot E_{50}^{u} \tag{7.4}$$

Factor f was chosen to 0.3 and E_{50}^{ref} is calculated according to equation 7.5, with the same assumptions for c' and m as before.

$$E_{50} = E_{50}^{ref} \left(\frac{\sigma'_3 + c\cot\varphi}{p^{ref} + c\cot\varphi} \right)^m \qquad (7.5)$$

The preconsolidation pressure, σ'_p are used for the minor effective stress, σ'_3, φ is the friction angle of the soil of 35°.The results can be seen in Figure 6.5 where E_{50}^{ref} is plotted vs. depth.

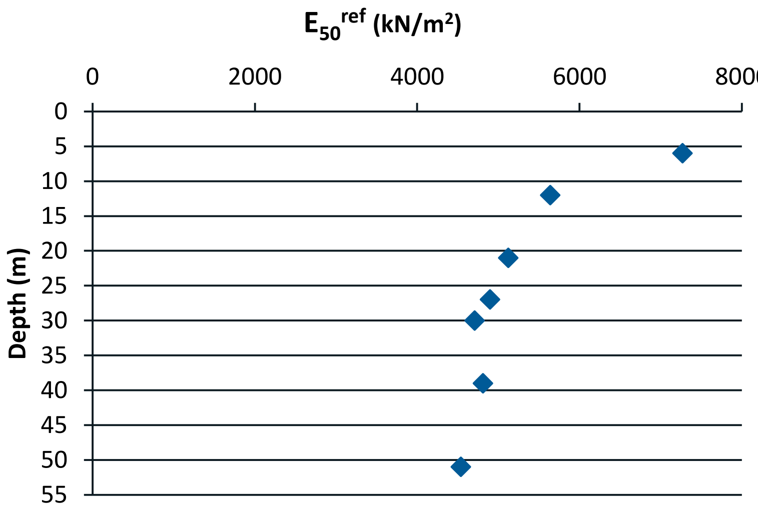

Figure 7.5 Values of E_{50}^{ref} over depth.

The remaining input values for the Hardening Soil model are collected directly from CRS and undrained triaxial test and are shown in Appendix B.1

7.1.1 Modified parameters for the Hardening Soil model

The parameters which were derived from laboratory test were used as input values for Hardening Soil model. The models stress-strain relationship is compared against the stress-strain relationship from the laboratory test. This is done to further calibrate the model parameters.

In the Hardening Soil model the function SoilTest tool was used, and the curve, produced by the model was compared with one from the laboratory tests. All four layers are compared to CK_0UC and CK_0UE. The input parameters from chapter 7.1 are then modified to fit the laboratory results better than the original ones. Figure 7.6 shows the curves from the laboratory tests, black curves, together with the curves generated by PLAXIS SoilTest, red curves, for an undrained triaxial compression test. The most important part to get a good fit of is the beginning of the curve up to its maximum deviatoric stress. From this stage the stress-strain curves are influenced by shear band and not used.

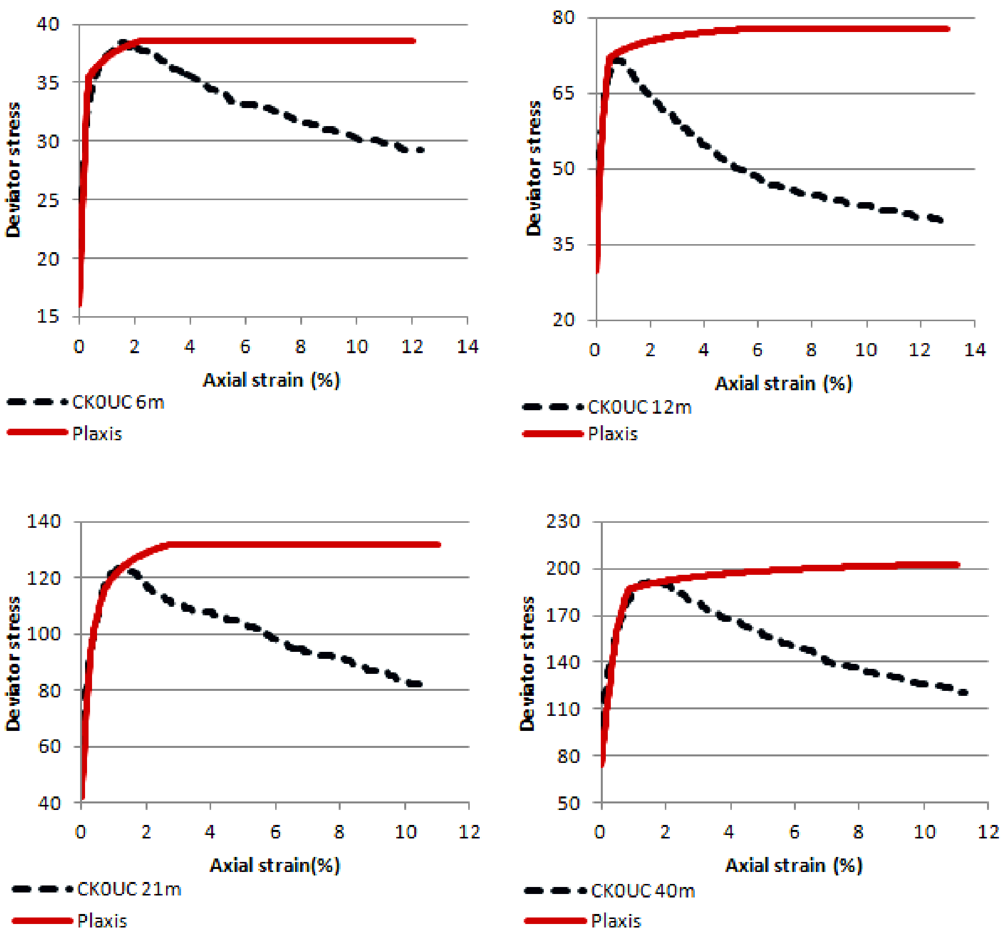

Figure 7.6 CK_0UC curves, fitted for Hardening soil model for different depths and layers. Black curve (dashed line) is from laboratory tests and red curve (solid line) is predicted by Hardening Soil model in PLAXIS tool SoilTest.

The corresponding stress paths for these tests in s'-t space can be seen in Figure 7.7

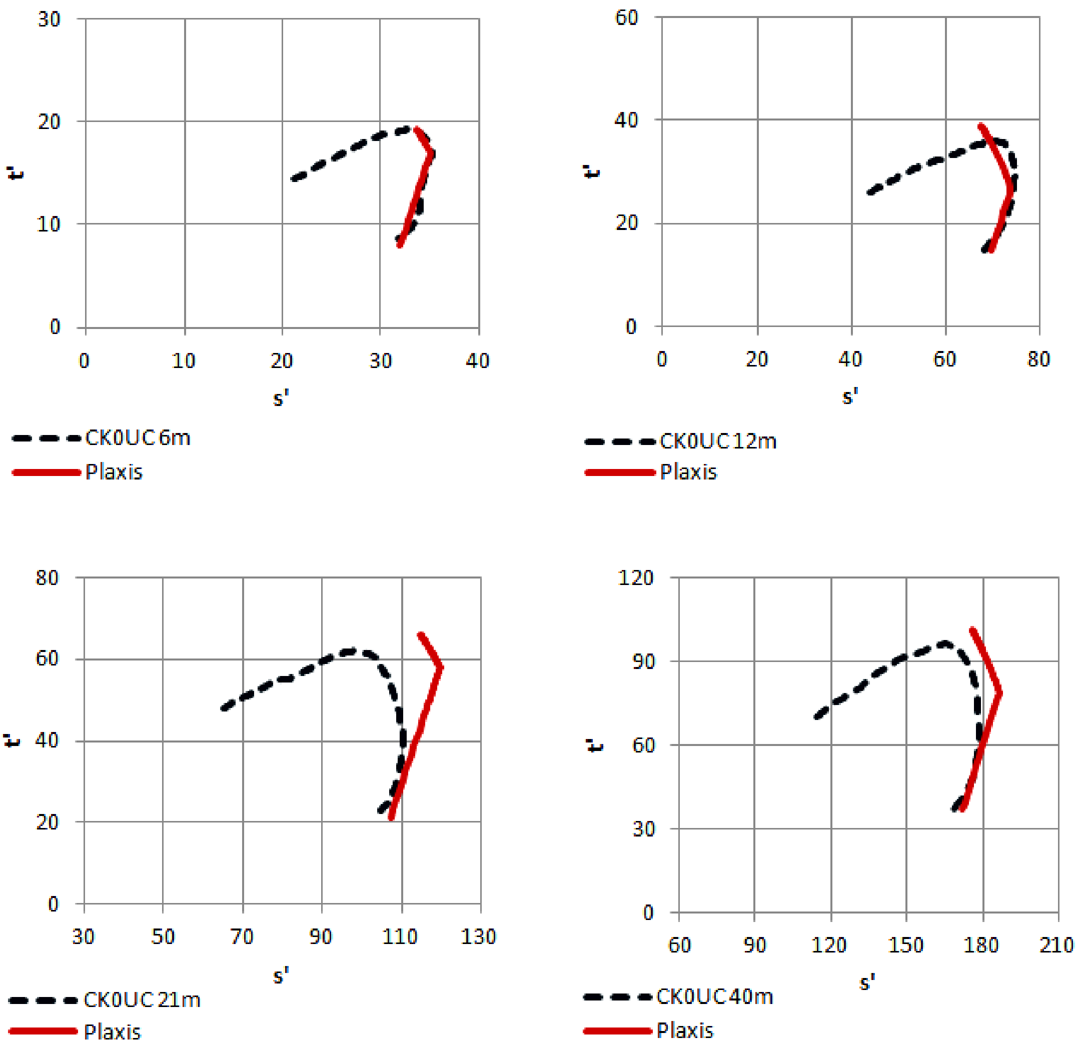

Figure 7.7 CK$_0$UC stress paths, fitted for Hardening soil model for different depths and layers. Black curve (dashed line) is from laboratory tests and red curve (solid line) is predicted by Hardening Soil model in PLAXIS tool SoilTest.

The modified parameters for the Hardening soil model are presented in Appendix B.2

A comparison with CK$_0$UE has also been performed but anisotropy influences this test and a good match is not possible in the Hardening Soil model, see Figure 7.9

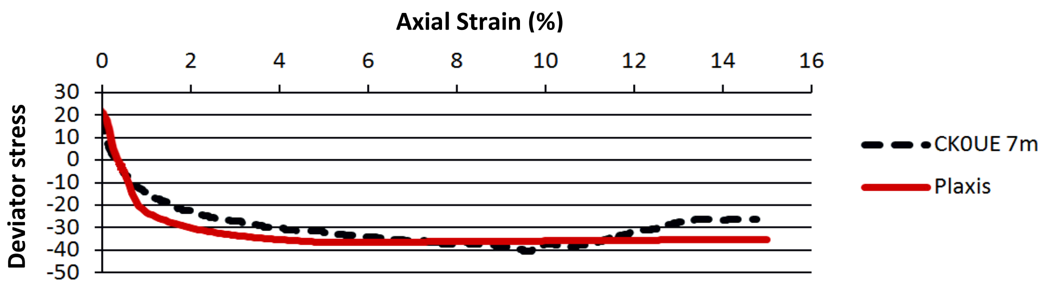

Figure 7.9 CK$_0$UE curve, fitted for Hardening soil model for 7 m depth. Black curve (dashed line) is from laboratory tests and red curve (solid line) is predicted by Hardening Soil model in PLAXIS tool SoilTest.

7.2 Parameters for the Creep S-CLAY1S model

The parameters for Creep-SCLAY1S are also derived from CRS oedometric test and undrained triaxial tests, however, some complementary oedometric test with stepwise loading are necessary for the creep and destructuration parameters. The procedures for deriving the parameters are described in the chapter below.

The modified compression λ* and swelling index κ* can be retrieved from an isotropic compression test and oedometric test. The slope of the normal consolidation line gives λ* and the slope of the unloading reloading line gives κ* in a plot with the logarithmic stress as a function of volumetric strain (Sivasithamparam N. , 2012).

$$\lambda^* = \frac{\lambda}{1+e} \tag{7.6}$$

$$\kappa^* = \frac{\kappa}{1+e} \tag{7.7}$$

$$\lambda^* = \frac{C_c}{2.3(1+e)} \tag{7.8}$$

$$\kappa^* = \frac{2C_s}{2.3(1+e)} \tag{7.9}$$

To obtain the parameters λ^* and κ^* several CRS oedometer test with unloading reloading procedures were used. The slope of the normal compression line and unloading reloading line were evaluated for the λ^* and κ^* values. The parameter λ_i^* is necessary if destructuration is taken into account. This value is obtained from an incremental oedometer test. This kind of test is not available for the investigated area and a test with typical data for Göteborg clay is used instead. The value is derived from an ln-stress: strain plot, where the slope in the end of the curve gives the value of λ_i^*, see Figure 2.2 in Section 2.1. Due to lack of data the same λ_i^* is used for all layers.

Poisson's ratio ν, is assumed to be low and the value of it is in the range of 0.1 and 0.3.

The critical state line M is based on the friction angle φ' and could be compared to Drucker-Pragers failure line which has a shape of a cone in principle stress space as described earlier. The critical state line can be obtained by the following equation 7.10

$$M = \frac{6 sin\varphi\prime}{3 - sin\varphi\prime} \tag{7.10}$$

In Creep-SCLAY1S is it possible to choose a critical value both for compression M_c and extension M_e. If they are chosen to be the same then the model will assume Drucker-Prager failure surface. The friction angle is chosen to 35° in compression and 38° in extension.

The initial inclination of the yield surface α_0 is defined by equation 7.11 and originally taken from Wheeler et al. (2003)

$$\alpha_0 = \frac{\eta_{K0}^2 + 3\eta_{K0} - M^2}{3} \tag{7.11}$$

The parameter M is the critical state line and η_{K0} is the normally consolidated stress ratio. The value of η_{K0} can be estimated from Jaky's formula K_0=1-sinφ' with the equation 6.12.

$$\eta_{K0} = \frac{sin\varphi\prime}{1-\frac{2}{3}sin\varphi\prime} \tag{7.12}$$

And with equation 7.12 it is possible to solve for α_0 in equation 7.11.

The parameter ω_d defines relative effectiveness of plastic volumetric and plastic shear strains in rotational hardening. Also this equation is from Wheeler et al. (2003) and formulated in equation 7.13

$$\omega_d = \frac{3(4M^2-4\eta_{K0}^2-3\eta_{K0})}{8(\eta_{K0}^2-M^2+2\eta_{K0})} \tag{7.13}$$

where M is the critical state line and η_{K0} is the normally consolidated stress ratio. The absolute rate of rotational hardening ω can be estimated with the parameters $\alpha_{0,}$ M, ω_d and λ^* with equation 7.14 from Leoni et al. (2008)

$$\omega = \frac{1}{\lambda^*} ln \frac{10M^2-2\alpha_0\omega_d}{M^2-2\alpha_0\omega_d} \tag{7.14}$$

This equation may with some parameter combinations become negative which is not physically correct, and the empirical law by Zentar et al. (2002) see equation 7.15, which can be used when negative values appear in equation 7.14.

$$\frac{10}{\lambda} \leq \omega \leq \frac{20}{\lambda} \tag{7.15}$$

where λ is the normal compression line in v:lnp' space. The value of the initial bonding χ_0 can be derived from a fall cone test were the sensitivity S_t has been measured. See equation 7.16 for an estimation of the initial bonding in the clay (Sivasithamparam, 2012).

$$\chi_0 \approx S_t - 1 \tag{7.16}$$

Figure 7.10 displays the sensitivity S_t in the soil profile over depth and the initial bonding χ_0 was calculated from Figure 7.10 to 19 with sensitivity in the soil of 20 in the top layers and to 12 in the bottom layers.

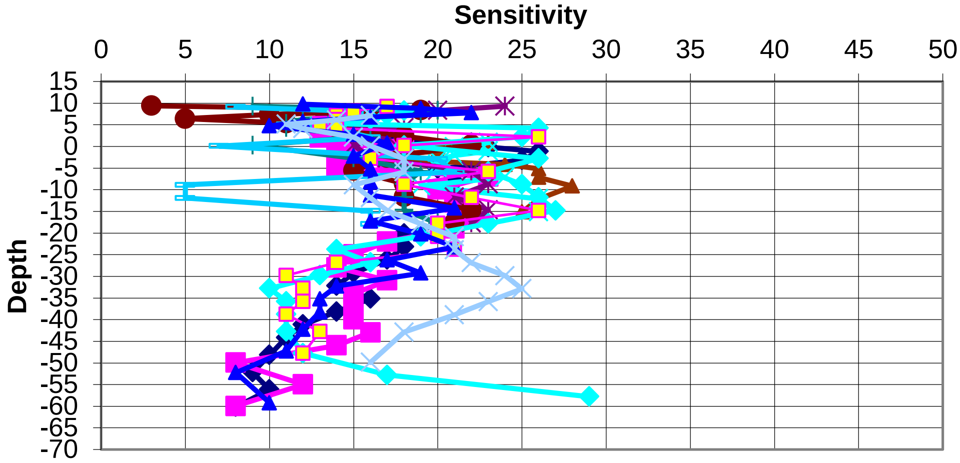

Figure 7.10 Sensitivity over depth. The different graphs are from different boreholes in the investigated area.

The reference time τ is linked to the preconsolidation pressure and is usually set to one day if the preconsolidation pressure is defined by 24h oedometer test (Brinkgreve et al. 2008).

The initial void ratio e_0 is defined by the volume of voids divided with the volume of solids. The void ratio is evaluated specific gravity of the soil and the water content and shown in Figure 7.11.

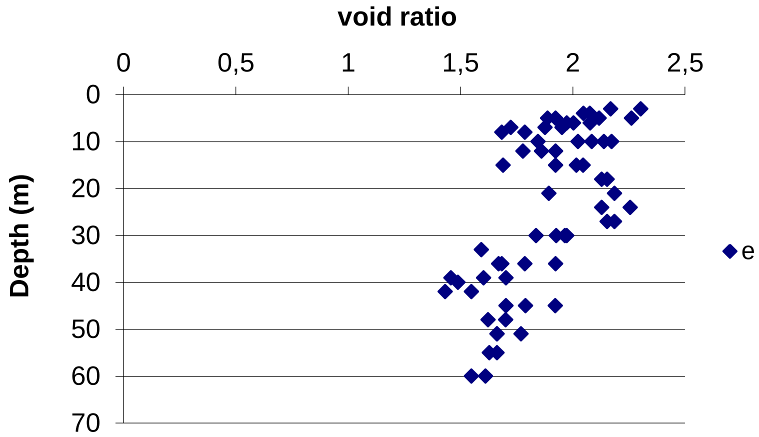

Figure 7.11 Void ratio over depth depth.

The value for absolute and relative rate of destructuration was suggested by Koskinen (2002). She suggested an optimisation procedure with modelling simulations of laboratory test to derive the parameters ξ and ξ_d. To obtain ξ Koskinen simulated drained triaxial tests with a low value of η. Due to the low value of η the stress path is close to isotropic and the shear strains are small so that the effect of ξ_d is negligible. The same procedure with high values of η is then performed for values of ξ_d (Krenn, 2008). As no such tests were available, typical values of 9 for ξ and 0.2 for ξ_d were used.

The modified creep index μ^* was obtained by plotting the long term volumetric strain against logarithmic time. This parameter is also derived from an incremental oedometric test and, therefore not obtained from data related to the investigated area. This value can also be derived from empirical data where $\alpha_{s,max}$ is obtained from the water content of the clay and the creep parameter μ^* is calculated from equation 7.17.

$$\mu^* = \frac{\alpha_{s,max}}{2.3} \qquad (7.17)$$

where $\alpha_{s,max}$ is a creep parameter from Swedish practice. The parameter of μ^* corresponded well to both methods with the same result. A table with all input values for Creep-SCLAY1S can be seen in Appendix C.1.

7.2.1 Modified parameters for the Creep-SCLAY1S model

The same procedure as mentioned in chapter 7.1 where the Hardening Soil models parameters were compared to laboratory test were performed for the Creep-SCLAY1S model. Also here SoilTest tool was used to simulate different tests. The tests that were simulated by Creep-SCLAY1S model were CK_0UC and CK_0UE. However, Creep-SCLAY1S did not work with SoilTest tool in PLAXIS version 2012. This was solved by using an older version of PLAXIS. The version that was used for this work was 2011, and the simulations worked as they should.

Figure 7.12 shows the comparison of the undrained triaxial compression tests from laboratory test in black and the simulated test from PLAXIS in red. Figure 7.13 shows the corresponding stress paths for the same tests in s'- t stress space. The test has been consolidated the same way in PLAXIS as in the laboratory and the strain rate is set to the normal rate in Sweden of 0.6% per hour. The fit of the curves were good in Figure 7.12 because only the first part of the curve is used.

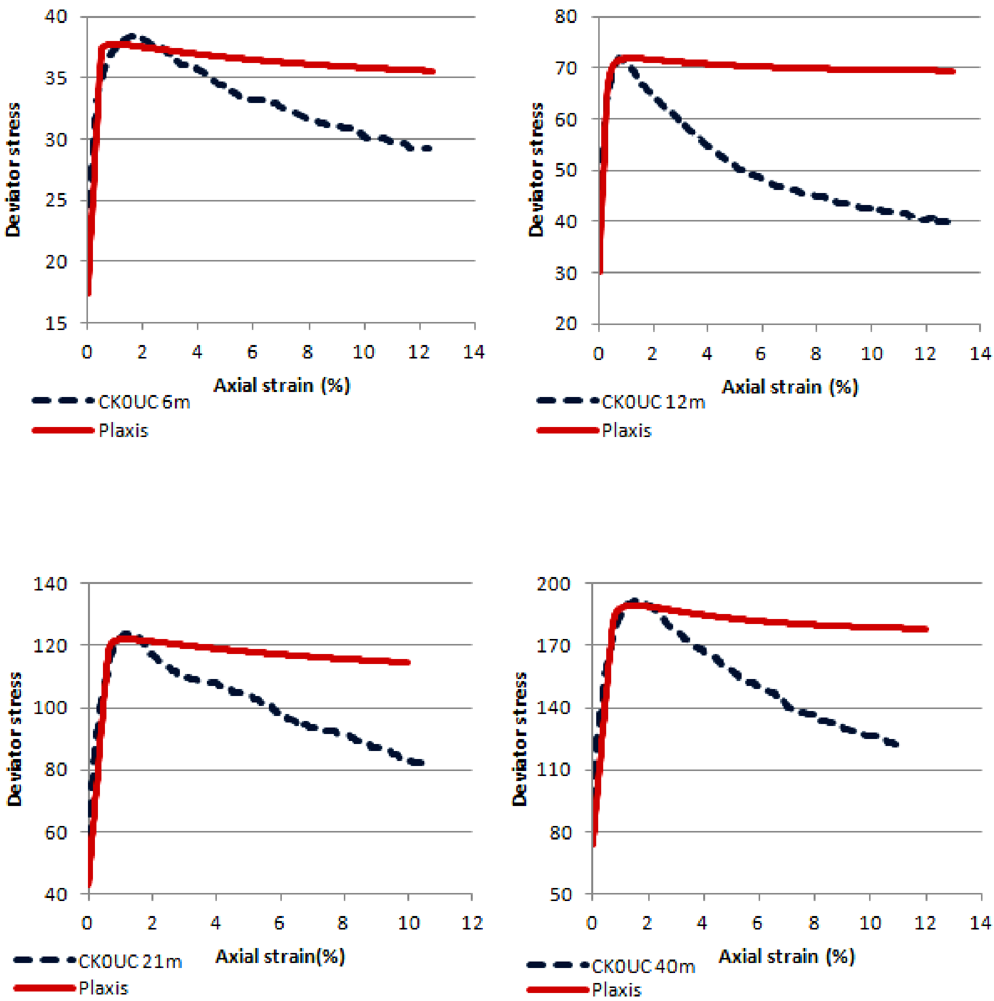

Figure 7.12 CK$_0$UC curves, fitted for Creep-SCLAY1S for different depths and layers. Black curve (dashed line) is from laboratory tests and red curve (solid line) is predicted by Creep-SCLAY1S in PLAXIS tool SoilTest.

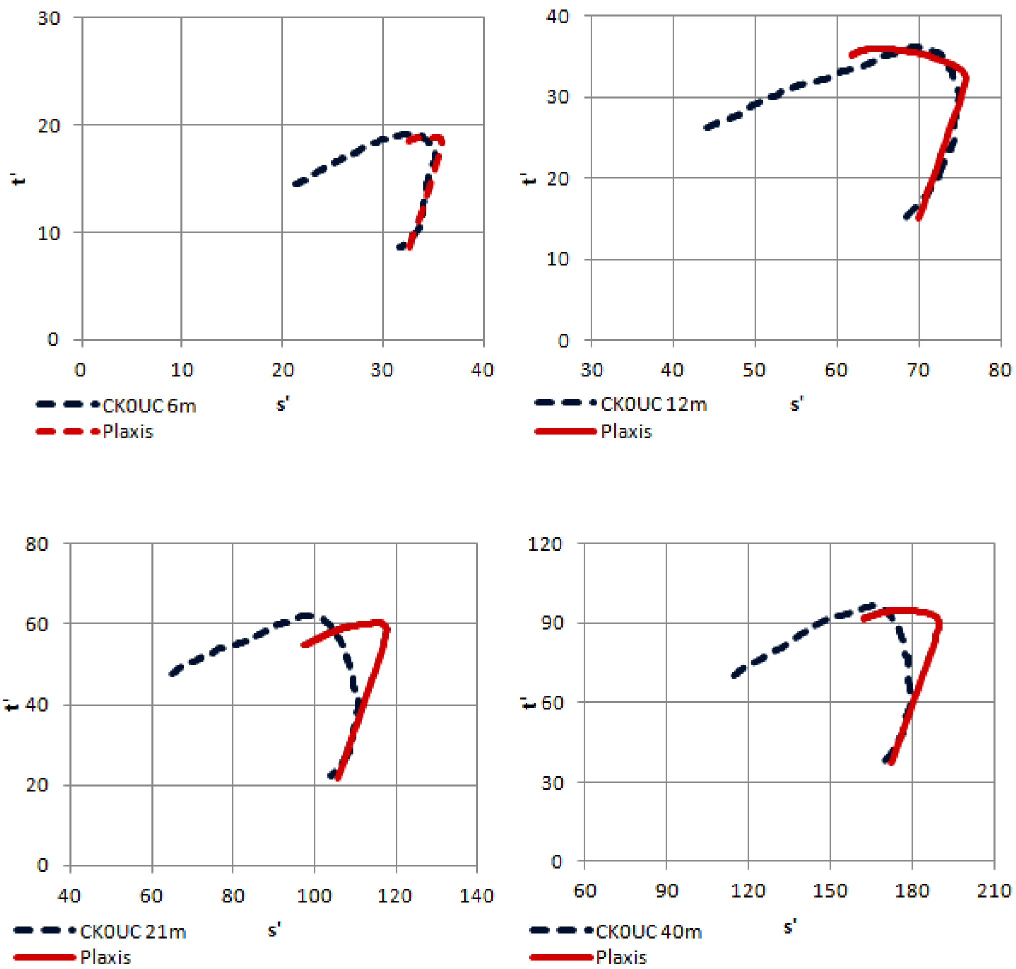

Figure 7.13 CK_0UC stress paths, fitted for Creep-SCLAY1S for different depths and layers. Black curve (dotted line) is from laboratory tests and red curve (solid line) is predicted by Creep-SCLAY1S in PLAXIS tool SoilTest.

It is however possible to get an even better match than the one in Figure 7.12 if the destructuration parameter χ_0 is used. This was turned off due to problems with consolidation when the parameter was modelled. The excess pore pressure continued to increase during consolidation, which could attributed to creep or Mandel Cryer effect. Mandel Cryer effect makes it is possible for pore pressure to increase inside of the soil to stresses greater than those that were externally applied. These will later on dissipate. (Gourvenec & Randolph, 2010). This phenomenon which is seen in the calculation phase is probably a consequence of the parameter set. It can either be that the clay is too sensitive to be represented by the model or because some values that are necessary for the destructuration such as λ_i^* is not from the investigated area. The results for all input parameters can be seen in Appendix C.2.

Figure 7.14 shows the results for the undrained triaxial extension tests and their corresponding stress path can be seen in Appendix C.3-C.4.

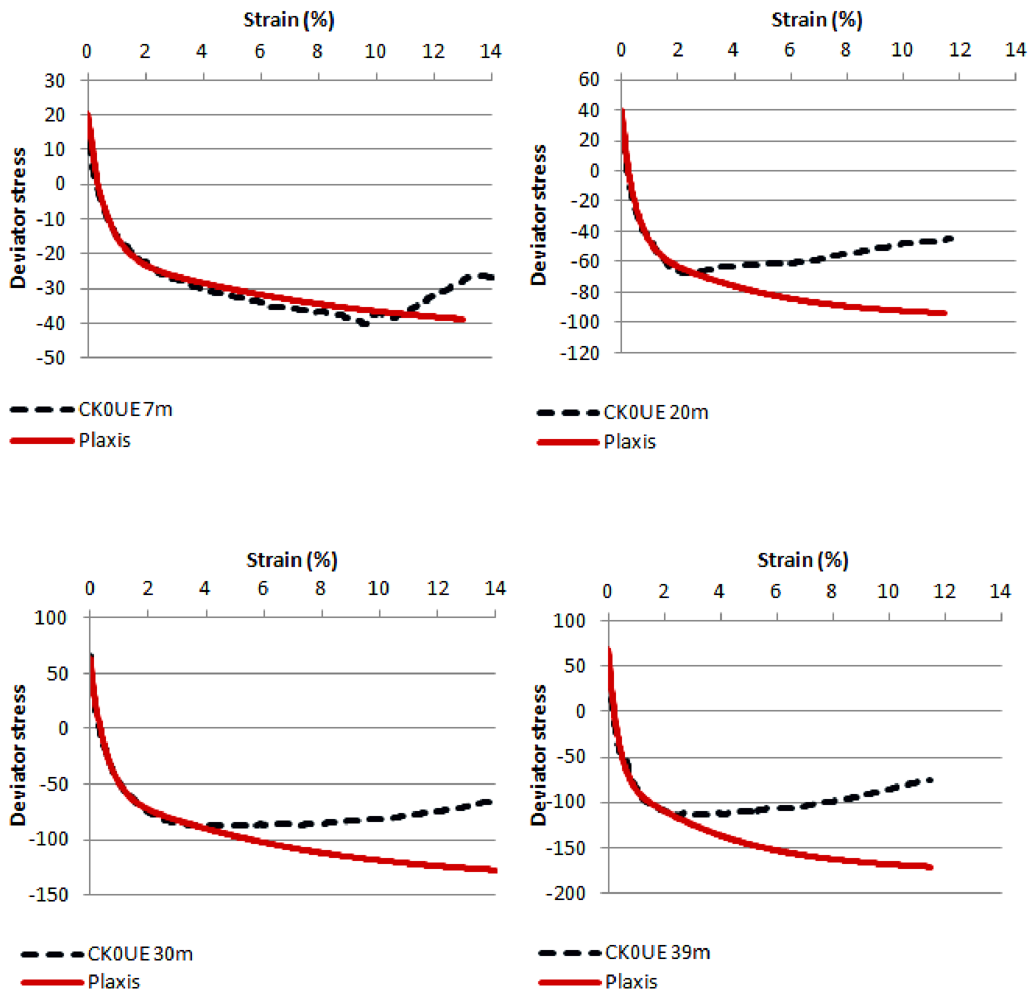

Figure 7.14 CK0UE curves, fitted for Creep-SCLAY1S user defined model for different depths and layers. Black curve is from laboratory tests and red curve are modelled in Hardening soil models application soil test.

Also these results would have a better match if the destructuration parameters had been taken into account. Compared to the Hardening soil model are these fits much better and because of that Creep-SCLAY1S accounts for anisotropy extension values can be used. This is an advantage for problems regarding excavations were the stress paths corresponds to these tests and not compression tests.

8 Modelling of Case

In this chapter three different cases will be described and results from them presented. The first case an excavation with a train load applied next to the excavation will be simulated. The main focus for this case is to investigate how long the excavation can stand open and to investigate how the dynamic train load influence the stability of the excavation with time. The second case is a deeper excavation than the first one but in this case is the train load removed. The focus on this case is how long the excavation can stand open until it the clay reaches creep rupture but also how this corresponds to the global factor of safety. The last case will investigate creep and creep rupture in a soil test, which is simulated by PLAXIS SoilTest tool. The focus is to see at which degree of mobilisation tertiary creep or creep rupture occur.

8.1 Case 1 – Excavation with train load

The first project investigated in this thesis was BanaVäg i Väst which was completed in December 2012. This project included a four lane motorway and a double track railway between Göteborg and Trollhättan, see Figure 8.1. The purpose of the project was to increase the safety and standard on the highway and to increase the amount of cargo trains on the railway.

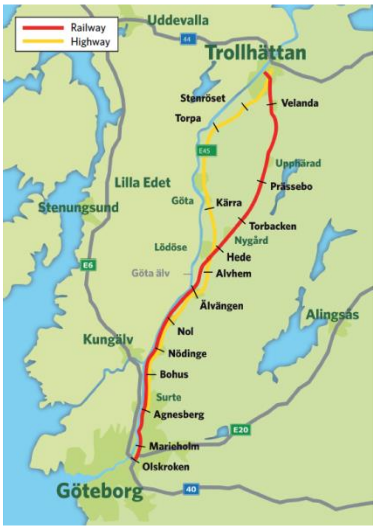

Figure 8.1 Stretch of BanaVäg i Väst (Trafikverket, 2013-03-25).

Skanska got the contract E33 which was located between Bohus and Nödinge. The contract included a railway of 3.2 km which was designed for velocities of 250 km/h. To meet this criterion there were high demands on the foundation of the railway. The ground condition was clay and to be able to reach the designed target values were lime cement columns installed along the stretch below a new embankment (Trafikverket, 2013-03-25).

The columns needed to be inspected and verified for the correct quality. The first meter of lime cement columns often have poor quality and because of that was the first meter excavated. The excavated material was replaced with fill material that became the subbase of the embankment. One part of the constructed stretch was close to an existing railway that was open during the construction period. It was uncertain if the excavation could be open when a train passed and to solve for this was a retaining structure installed and a staged excavation performed along the structure, see Figure 8.2. The procedure was repeated on the other railway track. Skanska Teknik was responsible for the temporary geotechnical structures in the project.

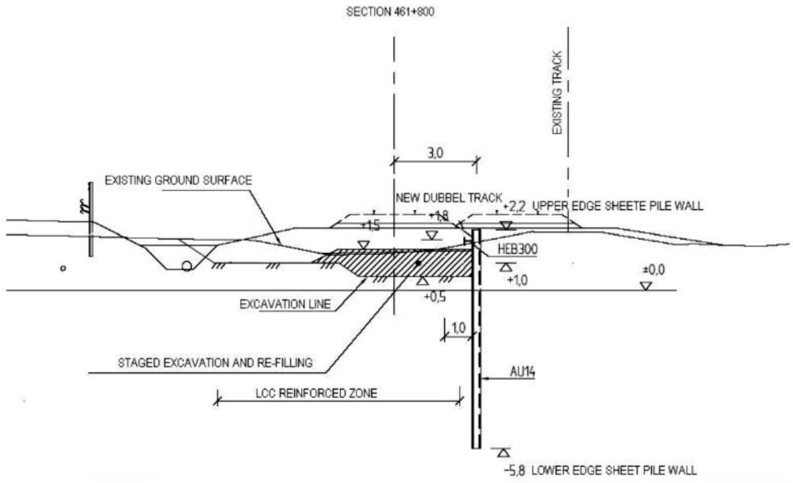

Figure 8.2 Cross section of the retaining structure and excavation next to the existing railway.

8.1.1 Geometry

The cross section in Figure 8.2 is simplified to the geometry seen in Figure 8.3. The geometry is modelled with four layers of clay based on the water content in the clay, see Appendix A.1 Each layer has its own stiffness parameters as shown in Section 7. At the top of the clay there is a dry crust which is 0.5 m deep. The dry crust is modelled with a Tresca model with undrained behaviour. The undrained shear strength is chosen to 40 kPa for this layer. The excavation is 1 m deep on the left side of the sheet pile wall and to the right side of the sheet pile wall there is an embankment. The embankment is modelled as a Mohr Coulomb model with fill material, the properties for the fill are shown in Appendix D.1 The distributed load on top of the embankment represents the train and has an input value of 44 kPa.

The sheet pile wall is modelled isotropic and its properties and input values are shown in Appendix D.2. An interface is installed around the sheet pile. The interface is a virtual thickness which is used to define material properties for the interface. The interface has the same properties as clay layer 1 but the material type is changed to be drained instead of undrained. This drained behaviour enables the gap between the soil and the sheet pile wall to be filled with water and water pressure develops against the wall.

All four clay layers are modelled as material type Undrained (A). When modelling undrained behaviour in PLAXIS excessive pore pressure develop during plastic stages when the total mean stress increases, and it is possible to perform an consolidation analysis after an undrained calculation due to that the undrained shear strength is an result of the model and not an input value.

The boundary conditions for the model are set by the standard fixities function. This function sets the vertical boundaries a horizontal fixity u_x=0 and the horizontal boundary are set to a full fixity $u_x = u_y = 0$. This means that the deformations in the bottom of the model cannot move in any direction while the vertical boundaries are free to move in the y- direction but unable to move in the x-direction.

The water pressure in the soil is also generated during the initial phase. The water level is set 0.5 m below ground level at +0.5 m due to the dry crust which is implemented in the model. The boundary conditions for the water pressure are closed, both in vertical and horizontal direction. The vertical boundaries are closed due to symmetry and the horizontal in the bottom of the clay are closed due to impermeable rock beneath. The density of the water is the default value of 10 kPa.

All input parameters for both models can be seen in Appendix B and C.

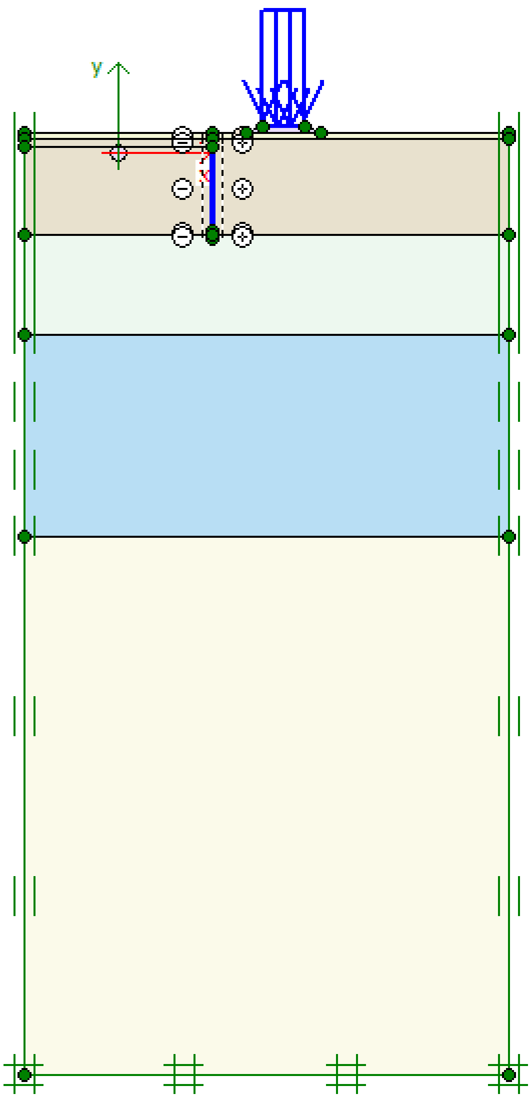

Figure 8.3 Schematic figure over the model in PLAXIS. It is the same geometry for both models, Hardening soil model and Creep-SCLAY1S

8.1.2 Calculation

The calculations are divided into six or seven phases depending on which model that are used. Only the last phase which is a safety calculation differs because it is not compatible in Creep-SCLAY1S because it is a User-defined model and not a standard. The calculation phases Case 1 are initial phase, installation of existing embankment, consolidation, installation of sheet pile wall, excavation, the train load is applied after the excavation as a distributed load and the last phase is a Safety analysis.

The first phase is the initial phase which is set to K_0-procedure. This procedure is chosen due to the horizontal ground and ground water level. In this phase is the initial stresses defined for the model were the loading history of the soil is taken into account. In the hardening soil model the default K_0 value is based on K_0^{nc} value but it is also influenced by either the OCR or the POP value. All initial layers are chosen in this stage to generate their stress levels.

The next phase is a plastic calculation with staged construction as a loading input. A plastic calculation is used for modelling of elastic plastic deformations where it is not necessary to take the decay of excessive pore pressures with time into account. In this phase is the embankment added on top of the dry crust. The hardening soil model does not take time into account but for Creep-SCLAY1S is one day chosen for the construction.

The next phase is a consolidation to minimum pore pressure at 2 kPa. This phase simulates a consolidations period of over 50 years. This ensures that the embankment already has settled after construction, this because it already existed for long time. The consolidation phase simulates dissipation of the excess pore pressure as a function of time. The excessive pore pressure that will be dissipated were generated from the last phase when the embankment was constructed. No additional geometry is defined in this stage and the loading input minimum pore pressure is used. This analysis is based on the excessive pore pressure and stops when the excess pore pressure is down to a specified minimum pore pressure parameter which was chosen to 2 kPa. No time interval can be chosen because the consolidation continues until it reaches the value of 2 kPa.

The next three phases are all plastic calculations with staged construction. The first of these phases is the installation of the sheet pile wall. Before this calculation begins are all deformations from the earlier stages deleted and the deformation starts over from this phase. The excavation is completed by deleting the area which simulates the excavation. In this phase are also the water conditions changed and the area for the excavation is modelled dry. Both the installation of the sheet pile wall and the excavation is performed in one day time. The last staged construction phase is the train load. In this phase the distributed load is turned on at 44 kPa. This trainload is varied for different time interval, 30 seconds, 1 hour and 1 day.

The last phase that is included in the Hardening Soil model is a safety calculation. This step calculates the global factor of safety for the project. In the safety calculation is the phi/c reduced until failure in the structure occurs. This cannot be completed in Creep-SCLAY1S because Mohr Coulomb's failure criterion is not included in the model and it is not one of the standard PLAXIS models.

The aim with Case 1 was to model an excavation with rate dependency in order to see how long it could stay open before it reached failure and also to see how trains that passes by influences the stability of the excavation. This was planned to be done by simulate creep over time. However calculations did not get that far because of some unexpected generated results. When the train load was applied in a plastic calculation phase large creep deformations occurred and these were varying with the time interval for that phase. A train load is a dynamic load and hence not there long enough to have significant effect on consolidation and creep. Figure 8.4 shows results generated from a train load which was applied under 30 seconds.

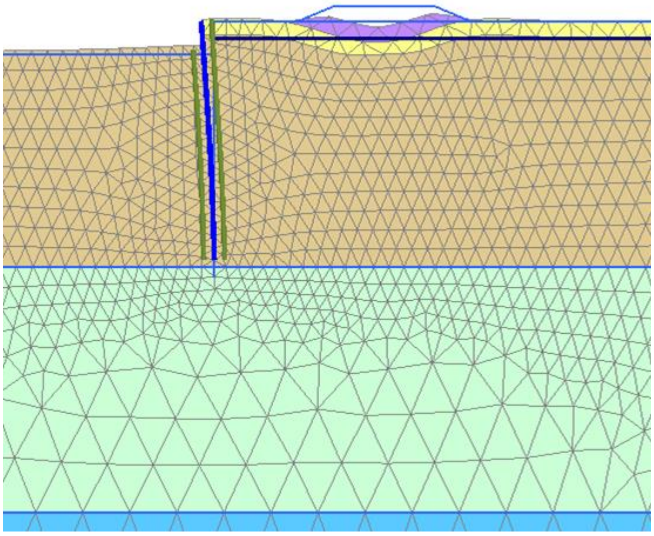

Figure 8.4 Deformation from train load after a time interval of 30 seconds (true scale).

Table 8.1 shows settlement below the train embankment after the applied train load for different time intervals. This effect was not expected from the beginning and no further analysis was conducted on Case 1 because of this.

Table 8.1 Settlements below the embankment generated after train load applied for different time intervals.

Train load (time interval)	Settlement (m)
30 s	0,612
1 hour	1,113
1 day	2,00

8.2 Case 2 – Excavation without train load

The applied train load in, Case 1 *Excavation with train load*, resulted in unrealistic deformations below the train embankment, see Section 8. A new hypothetic case was used to observe the rate effects influences an excavation using the Creep-SCLAY1S model. The main focus for this case was to observe how creep influences the stability of an excavation over time and when creep rupture occurs but also how this corresponds to the factor of safety. A simple geometry with an excavation depth of

2.5 m was chosen and the trainload was removed. The model in this case was chosen to be smaller to decrease the time of the calculations.

8.2.1 Hardening soil model

With a constant depth of the excavation a certain length of the sheet pile wall will correspond to a factor of safety. To find both the length of the sheet pile wall and its corresponding safety factor the geometry was implemented in the Hardening soil model.

Only one layer of clay was used, modelled as Undrained (A). The properties were collected from the modified values for the Hardening soil model Clay Layer 2 in Appendix B.2. The same boundary conditions were applied as in the previous section. It is assumed that the excavation is undrained, therefore the water level was set to ground level and generated by phreatic levels, which gives a hydrostatic pressure of water throughout the model. The interface is modelled using the same material parameters as for the clay except for using Drained behaviour. This ensures that water can fill the gap between the clay and the wall.

First, the initial state was generated the same way as in Case 1, see chapter 8.1. After this the sheet pile wall was installed and the excavation was performed. Both these steps used plastic calculations with staged construction. The global factor of safety was calculated by a safety calculation, phi/c reduction in the end of the excavation. This safety calculation uses the traditional system to calculate the factor of safety. This system accounts for uncertainties in the soil condition and ensures that deformations are small enough (Craig, 2004). Several factors of safety was searched for and the corresponding length of the sheet pile wall was found for these, see table 8.2

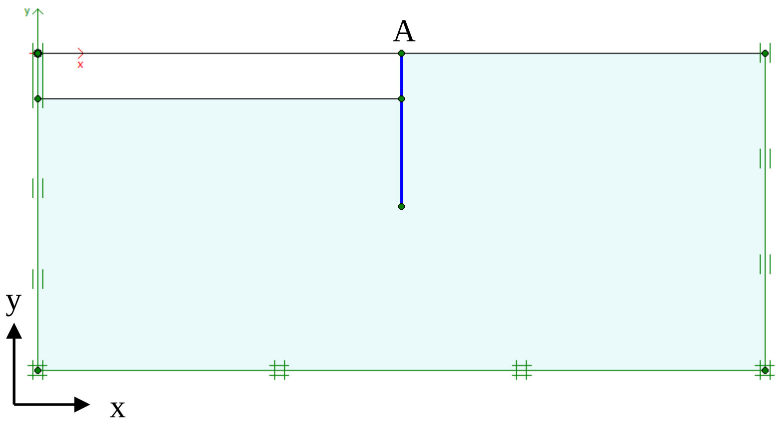

Figure 8.5 Geometry of the Case 2 - Excavation without train load.

Table 8.2 presents the global factor of safety attained for different wall lengths. Here is also the factor of safety, converted into the degree of mobilization, presented. The degree of mobilization is defined as the ratio of the stress state of the soil related to undrained shear strength of the soil determined with regular strain rates (Larsson, 1977), and calculated as the reciprocal of the global factor of safety. The geometry for the case with a 10.5 m long sheet pile wall is illustrated in Figure 8.5. This corresponds to a global factor of safety of 1.5 based on undrained shear strength simulated by the Hardening Soil model.

Table 8.2 Global factor of safety for the excavation using different lengths of the sheet pile wall.

Global factor of safety for the excavation	Length of sheet pile wall (m)	Degree of mobilization (%)
1.5	10.5	67
1.4	9.8	71
1.3	9.2	77
1.2	8.8	83
1.1	8.4	91
1.0	8.0	1

Finally the ultimate limit state was tested for the excavation with a safety factor of 1.5. The maximum load the excavation could withstand was calculated by applying a 1kPa distributed load at the top of the excavation. This load was increased until failure. This critical load was calculated to be 10.9 kPa. The failure mechanism of the wall was checked and shown in Figure 8.6. The failure mechanism is rotation around a point above the bottom of the sheet pile wall which could be expected by a cantilever wall.

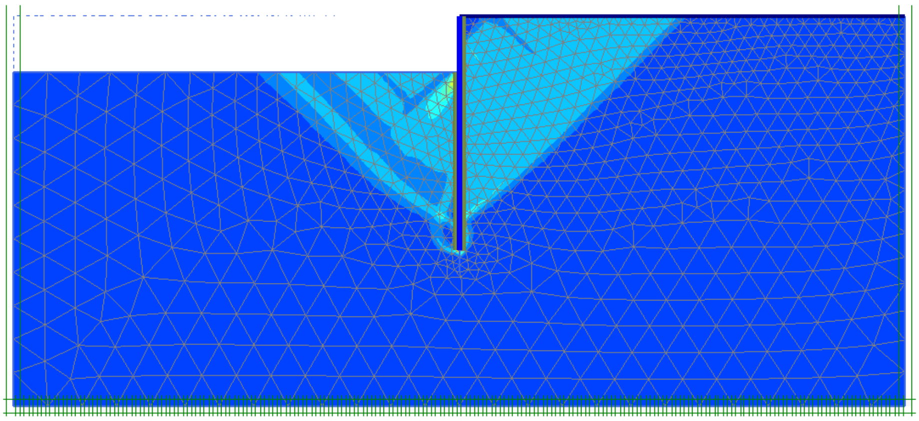

Figure 8.6 Schematic figure showing the failure mechanism for the wall in incremental strains for the Hardening soil model. The failure mechanism is a rotation around a point above the bottom of the excavation.

8.2.2 Creep and parametric study

Using the same geometry as in the previous section, but disregarding the load for the ultimate limit state, the creep was investigated. Note that the parameter values from Appendix C.2 were now chosen for the Creep-SCLAY1S model and that no interface is used. The interface was removed because it leads to unrealistic deformation results at the excavation. This suggests that there are problem with modelling interfaces when using user-defined models in PLAXIS. In one case the wall was displaced 0.5m while the clay still remained at its initial location. All phases in Creep-SCLAY1S are time dependent, and the installation time of the sheet pile wall and the excavation was set to 1 day each.

For the Creep-SCLAY1S model an undrained plastic calculation phase was added after the excavation. This was in order to investigate how the creep influenced the excavation. No changes to the geometry were made in this phase and the difference between the deformation directly after excavation and the undrained plastic phase are due to creep. The undrained plastic phase was modelled for 180 days. Figure 8.7 shows where the failure mechanism is after 180 days in the undrained plastic phase for Creep-SCLAY1S. Compared with Figure 8.6, both models have the same failure mechanism which also is correct to theory for a cantilever wall.

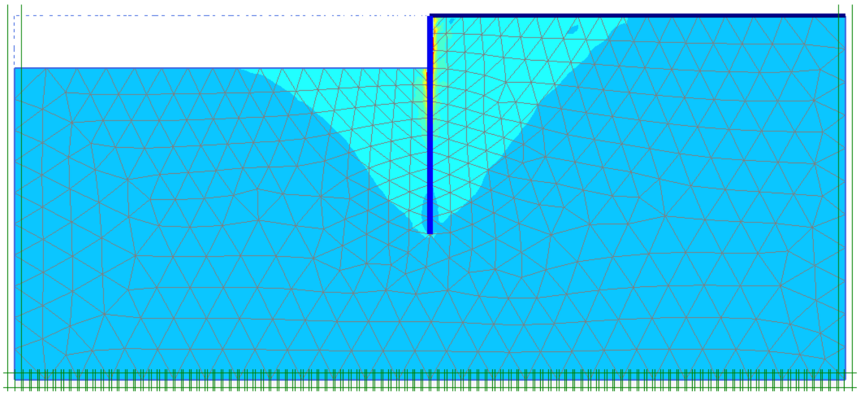

Figure 8.6 Schematic figure showing the failure mechanism for the wall in incremental strains for Creep-SCLAY1S. The failure mechanism is a rotation around a point above the bottom of the excavation.

Different lengths of the sheet pile wall with corresponding safety factor for the Hardening Soil model were presented in Table 8.2. The excavation has been modelled for different factors of safety, and the deformation in x-direction this resulted in is presented in Figure 8.8 where the global factor of safety is plotted as a function of deformation of point A (see Figure 8.5) directly after the excavation (red dashed curve) and after 180 days in the plastic undrained phase (blue solid line). Empirical data from Skanska Teknik is that a normal restriction when designing a retaining wall is an allowed movement of the wall is 5-10 cm.

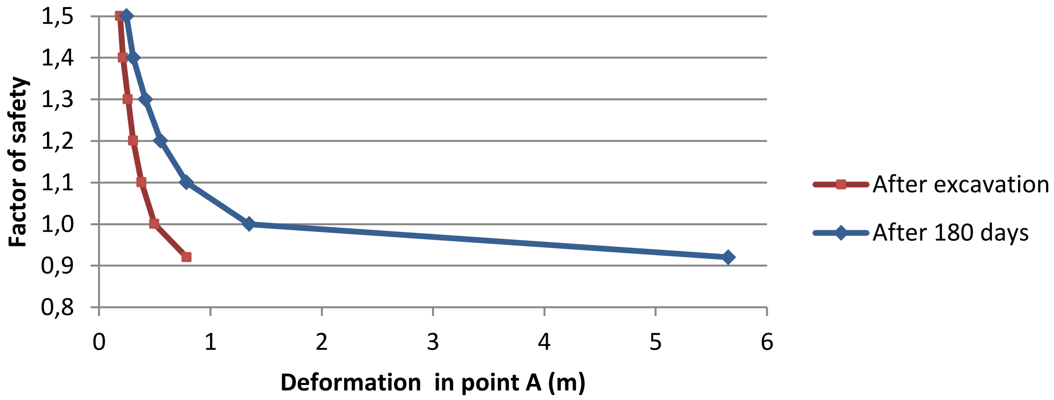

Figure 8.8 Global factor of safety over deformation after 180 days in undrained conditions.

From Figure 8.8 it can be seen that a lower global factor of safety leads to larger deformations, and most of it is caused by creep. The same phenomenon is seen in Figure 8.9 where the deformation in point A is plotted as a function of time. Here it can be seen that the increase in deformation is quicker for lower global factors of safety, however, no tertiary creep can be seen in any of the cases. It is also possible to see how large part of the deformation comes from creep and how much of it that is because of the excavation. The deformation from the excavation is seen until day two and all deformation from that day are due to creep, but some creep is still occurring during the excavation.

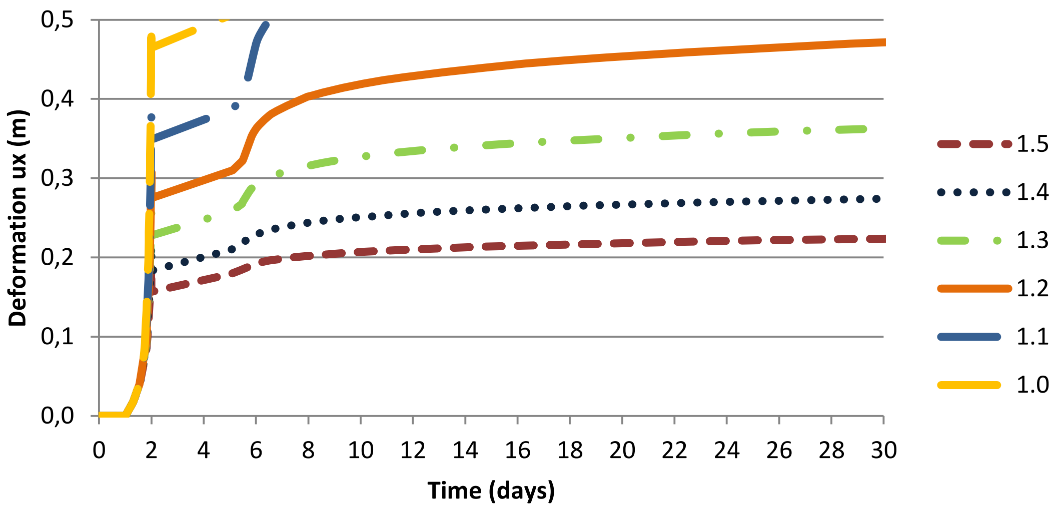

Figure 8.9Deformation over time with different factors of safety. The deformation is in x-direction from point A, in the top of the sheet pile wall (see Figure 8.5).

However, according to the test by Larsson (1977) tertiary creep should develop around a safety factor of 1.25, corresponding to a degree of mobilization of 80%. Now, for evolution of tertiary creep in Creep-SCLAY1S destructuration χ_0 must be switched on. The data presented above was calculated without destructuration due to the problems described in Section 7.2.

To be able to catch tertiary creep destructuration χ_0 was now turned on. With a destructuration parameter $\chi_0 = 19$ the remaining model parameters were modified to fit the undrained triaxial compression test, see table 8.3 for input parameters. Figure 8.11 below shows the match of the fitted parameter set with activated destructuration to laboratory test CK_0UC, note that λ^* is replaced by λ_i^*. The fitted parameters may be found in Table 8.3 below, hereafter referred to as parameter set 1.

Having fitted the parameters, the simulation with destructuration was performed for a global factor of safety of 1.5. Figure 8.10 show the deformation over time for this calculation. Here the sheet pile wall is installed during day one, no deformation is seen until the excavation, day two. From day two the simulation is in the plastic undrained phase with no changes to the geometry, the only deformation is caused by creep. Note the acceleration of deformation after 17 days. This is the tertiary creep where the stress path for the soil has passed the failure line. However, according to Larsson (1977) this behaviour should not occur until a mobilization degree of 80%. Since a safety factor of 1.5, or mobilization degree of 67%, was used the effect is unexpected.

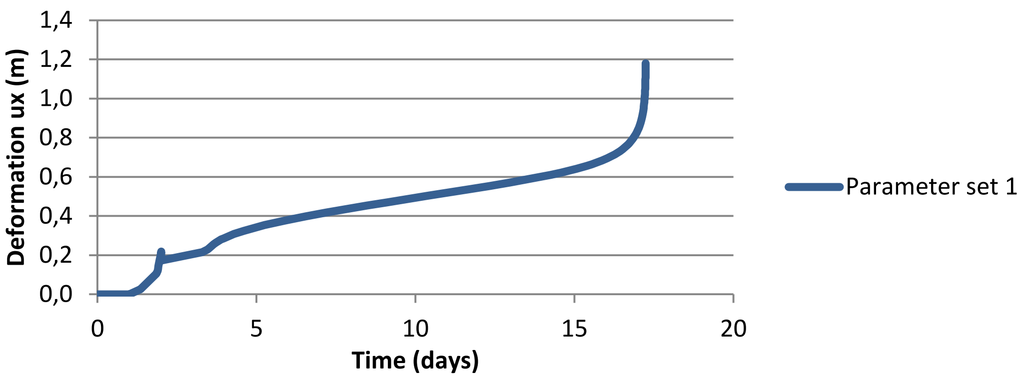

Figure 8.10 Deformation for A over time for a case with factor of safety of 1.5, χ_0 = 19.

The largest uncertainties when the parameters were chosen in Section 7 were in the parameters μ^* and λ_i^*. This was due to lack of data from an incremental oedometer test. The values were instead chosen based on data collected from another area with typical Göteborg clay. However, the value of λ_i^* is large compared to values reported for other Scandinavia clays (Karstunen et. al, 2005).

Therefore all parameters were matched again, this time using the smaller value of λ_i^*=0.12 instead of 0.22. This fitted parameter set is hereafter referred to as parameter set 2. Figure 8.12 show the fitted curves and the parameters are presented in Table 8.3 Note that, to be able to match with the smaller λ_i^*, μ^* had to be decreased.

Table 8.3 Parameters used for the two fitted parameter sets.

	Parameter set 1 - Clay layer 2	**Parameter set 2 – Clay layer 2**
κ*	0,015	0,015
ν'	0,2	0,2
λ_i*	0,22	0,12
M_c	1,42	1,42
M_e	1,55	1,55
ω	25,00	25,00
ωd	0,96	0,96
ξ	9	9
ξd	0,2	0,2
OCR	1,26	1,26
e_0	1,75	1,75
α_0	0,50	0,50
χ_0	19	19
τ	1	1
μ*	0,003	0,001
K0	0,647	0,647

Figure 8.11 show a comparison between the deformation results for calculations using parameter sets 1 and 2 respectively, still using a global safety factor of 1.5. Note that the result for parameter set 1 is the same as presented in Figure 8.11 but now plotted for a longer time period. When using the new parameters no creep failure occurred during the simulated 180 days. However the clay is still creeping at the end of the simulation period.

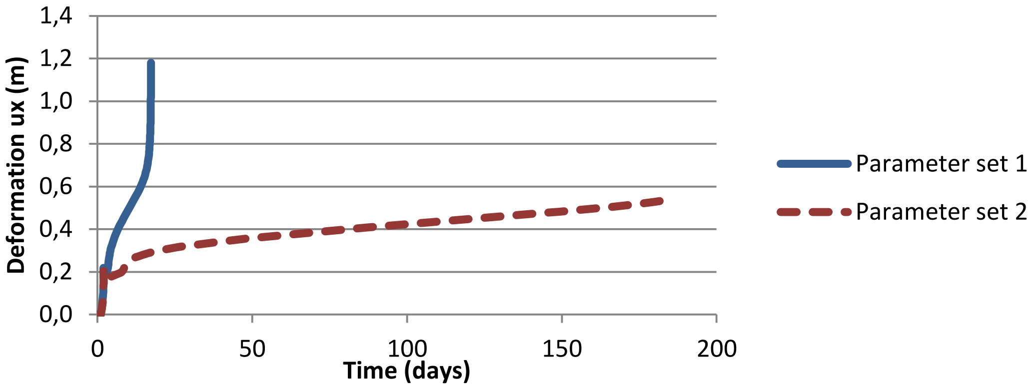

Figure 8.11 Deformation over time for an excavation with global safety factor of 1.5 using the two different parameter sets.

Figures 8.12 and 8.13 show the fitted curves for parameter sets 1 and 2. Both fit the data well, only the beginning of the stress-strain curve are used, see Section 7, and it is hard to find any graphical differences between the two sets. However, as discussed above, the change of μ^* and λ_i^* result in very different deformation results as shown in Figure 8.11.

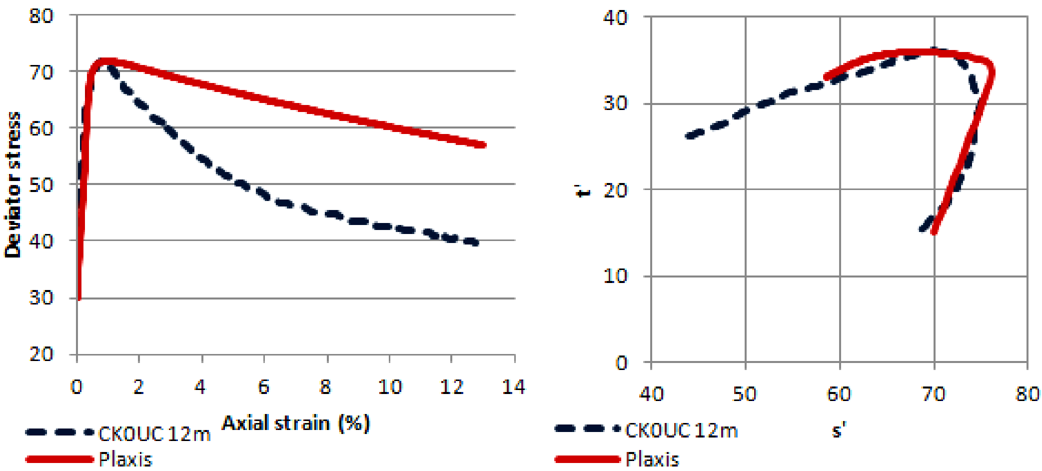

Figure 8.12 CK_0UC curve, fitted for Creep-SCLAY1S for clay layer 2, parameter set 1. Black curve (dashed line) is from laboratory tests and red curve (solid line) is predicted by Creep-SCLAY1S in PLAXIS tool SoilTest.

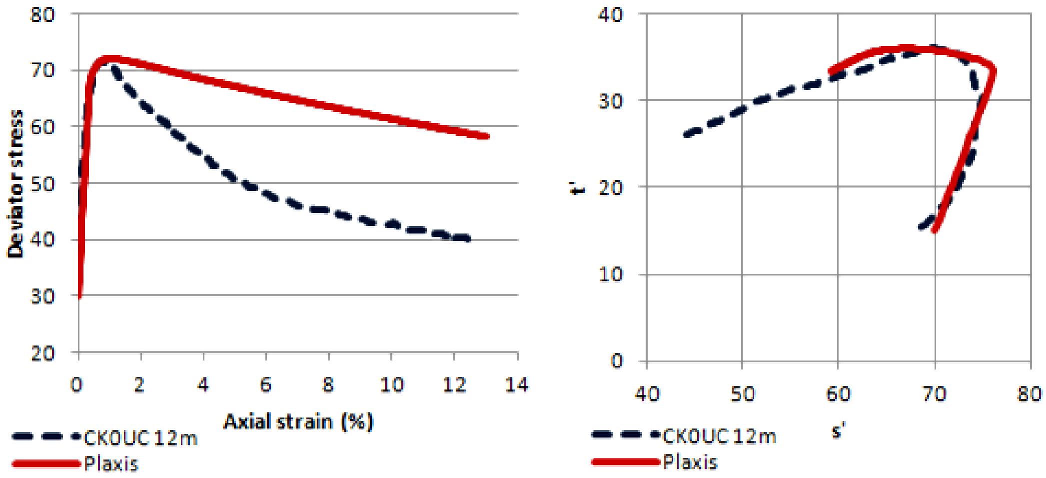

Figure 8.13 CK_0UC curve, fitted for Creep-SCLAY1S for clay layer 2, parameter set 2. Black curve (dashed line) is from laboratory tests and red curve (solid line) is predicted by Creep-SCLAY1S in PLAXIS tool SoilTest.

Using parameter set 2 the excavation was simulated for four different global factors of safety, presented in Figure 8.14. For a global factor of safety of 1.3 and 1.4 failure occurred six and nine days after the completed excavation respectively and for a global factor of safety of 1.2, creep failure occurred during the construction of the excavation. The results show the same trend as Larsson found in his laboratory tests (Larsson, 1977), even if it is for smaller degrees of mobilization using the Creep-SCLAY1S model. For parameter set 1 tertiary creep starts from a degree of mobilisation of 67, probably even lower, and for parameter set 2, tertiary creep starts from 71 % degree of mobilization. However, the results this far shows that the transition into tertiary creep is sensitive to some input parameters.

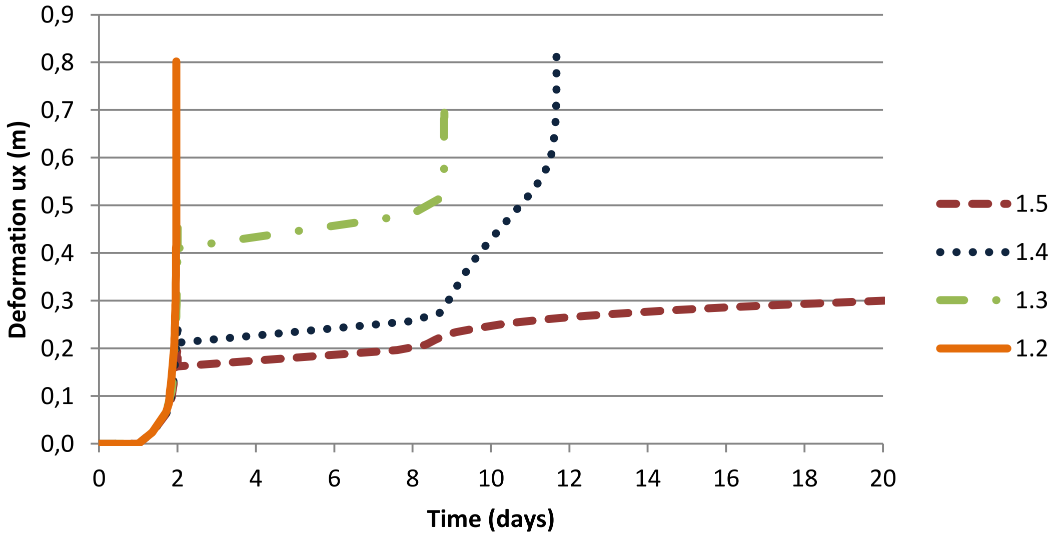

Figure 8.14 Deformation over time for different global factor of safety using parameter set 2.

Either which parameter set that is used it is clear that there need to be restrictions for tertiary creep when designing retaining walls.

To investigate how creep affects the behaviour of the clay next to the sheet pile wall the earth pressure on the passive and active side of the sheet pile wall is investigated. Figure 8.15 shows the earth pressure on the passive side against the retaining wall. The green triangles show the pressure directly after the excavation, the blue squares the pressure 7 days after the excavation and the red cubes 180 days after excavation. Figure 8.16 shows the pressure on the active side.

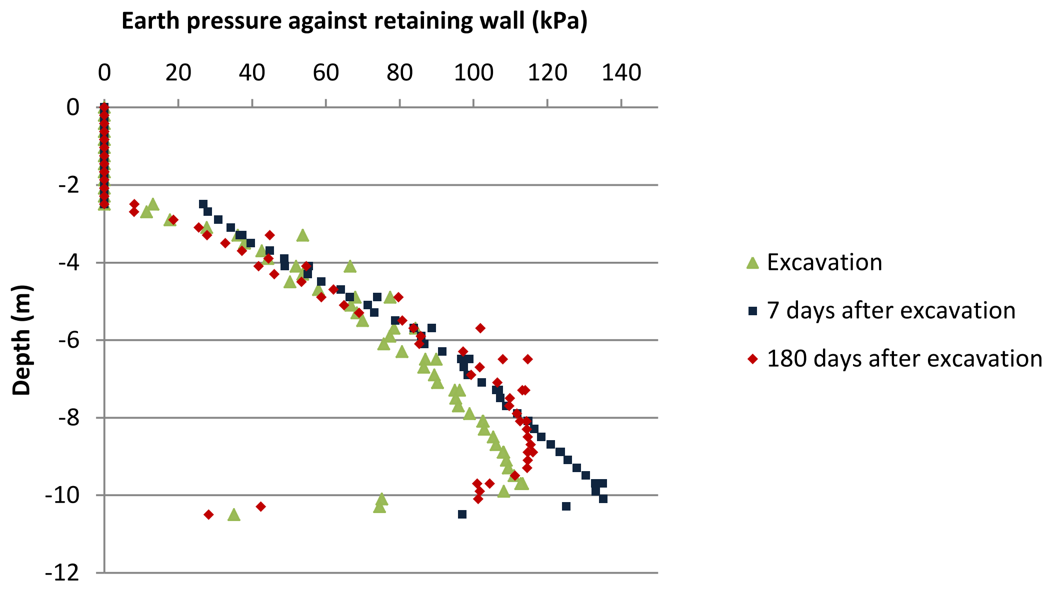

Figure 8.15 Earth pressure on the passive side of the retaining wall over depth.

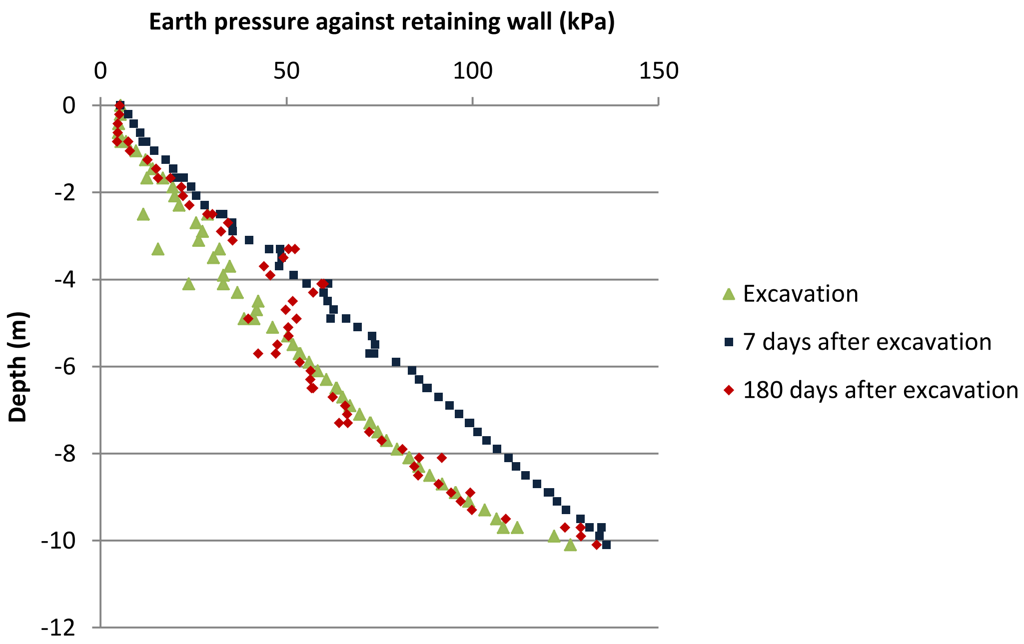

Figure 8.16 Earth pressure on the active side of the retaining wall over depth.

The behaviour of the soil next to the excavation is influenced by creep as seen in the presented Figures. In this process are there two different mechanisms working against each other. The already mentioned creep is one of them, this is easiest to see after seven days and the earth pressure against the retaining wall is the largest. The other mechanism is due to the rotation of the wall. This rotation decreases the earth pressure at the active side and the active pressure decreases. In Figure 8.17 a sudden change is apparent at 4 m depth, the same as the one seen for four meters depth in Figure 8.16. One theory of this could be that the soil has reached failure state but it could also be a local mesh dependent problem because no interface is used when Creep-SCLAY1S is modelled.

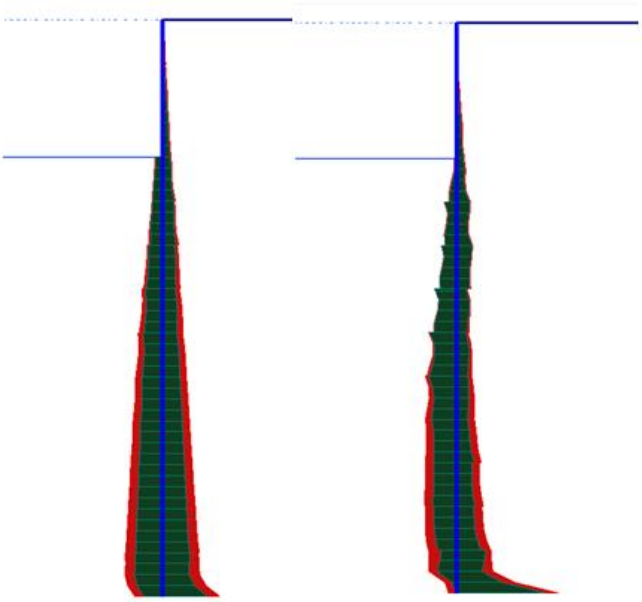

Figure 8.17 Total stress distribution of the retaining wall. The red area is water pressure and the green area is normal stress. The figure to the left is taken 7 days after the excavation and the figure to the right 180 days after excavation.

The peak in the lower end in the right of the pictures in Figure 8.16 could be because of rotation of the cantilever wall, after creep, and this pressure acts on the passive side instead.

8.2.3 Comparison of Hardening soil model and Creep-SCLAY1S

The initial settlements due to the excavation are presented in Figure 8.18. Settlements for both parameter sets using the Creep-SCLAY1S model is presented over time together with the settlements from the Hardening soil model. The plastic stage after day two includes no creep in the Hardening soil model and the deformation is as expected constant. The Creep-SCLAY1S model predicts a sudden drop in deformation in the beginning of the plastic undrained phase which cannot be explained.

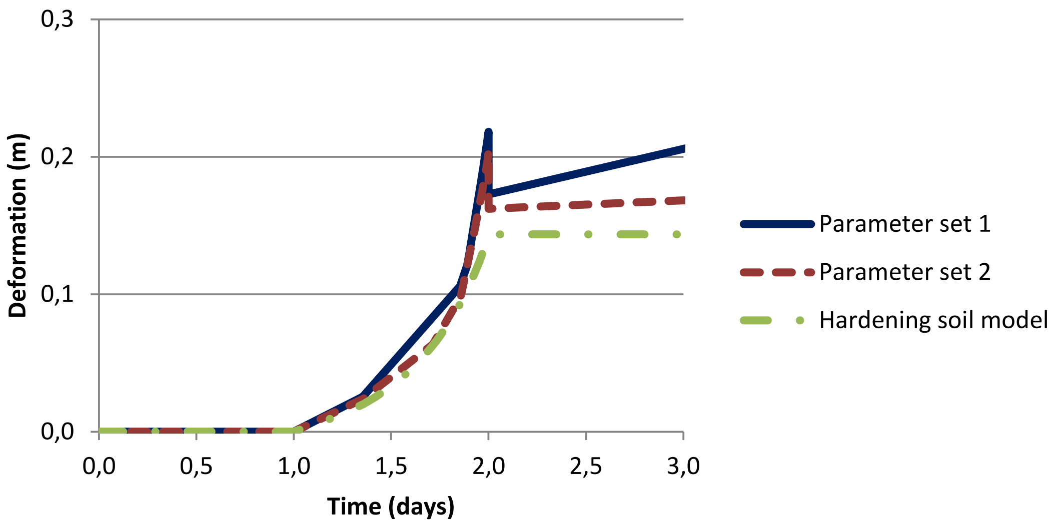

Figure 8.18 Deformations, in x-direction, during excavation and after for parameter sets 1 and 2 using the Creep-SCLAY1S model and for the Hardening Soil model. An excavation of 2.5 m with a global factor of safety of 1.5 is used. The deformation is plotted from point A (in Figure 8.5) over time.

According to the design directions, with an allowed movement of 5-10 cm of the wall, mentioned earlier in this section, the deformations from these models are all too high, already at the construction of the excavation. The settlement in y-direction is shown for both models in Figure 8.19. These are plotted from a point one meter to the right side of point A on the sheet pile wall over time.

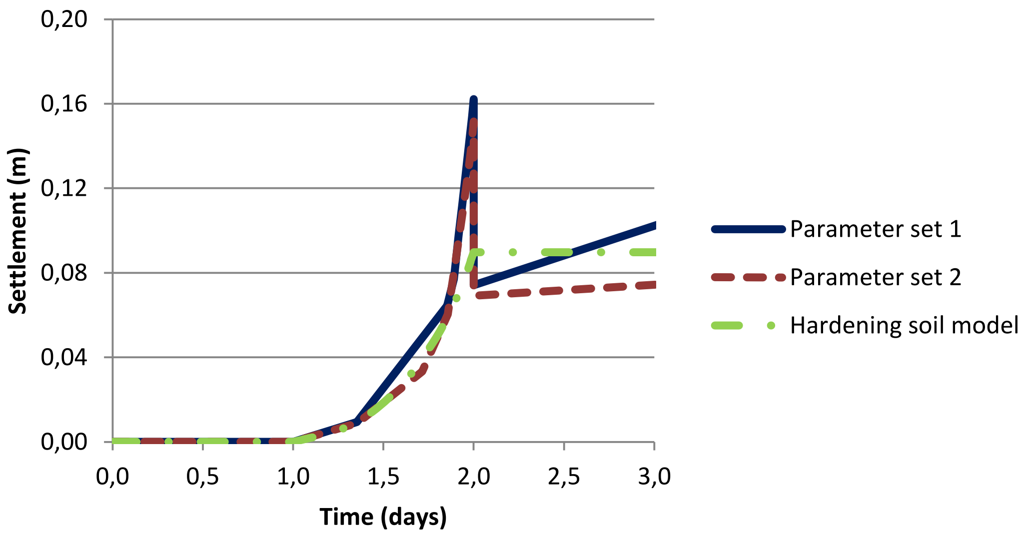

Figure 8.19 Deformation during excavation and after for parameter sets 1 and 2 using the Creep-SCLAY1S model and for the Hardening Soil model. An excavation of 2.5 m with a global factor of safety of 1.5 is used. The deformation is plotted 1 m to the right side of point A (in Figure 8.5) over time.

Appendix E show deformations for the Hardening soil model and Creep-SCLAY1S for parameter set 2. The deformations are presented directly after the excavation and

180 days after completed excavation for the creep-model. Forces in the structural element are presented in table 8.4 below.

Table 8.4 Maximum bending moment and shear forces on the sheet pile wall from both models are presented in the table.

	Hardening soil model	**Creep-SCLAY1S - Parameter set 2**	
		Directly after excavation	**180 days after excavation**
Maximum bending moment	113.7	121.5	182.8
Maximum shear force	34.1	35.4	52.2
Minimum shear force	-36.0	-48.5	-81

From table 8.4 it can be seen that the forces on the retaining structure are in the same range for both models before the creep evolves, but are increasing in the Creep-SCLAY1S model with time. The small difference in the first case directly after the excavation could depend on that there are no interface used in Creep-SCLAY1S but also that some creep occurs during the excavation.

8.3 Case 3 – Creep in Triaxial Compression Tests

In previous chapter tertiary creep were found for degrees of mobilization that were too low. Some uncertainties of the global factor of safety exists and to find for which degree of mobilization tertiary creep really starts for the two parameter sets were a undrained triaxial compression test with creep simulated with PLAXIS tool SoilTest. The test was simulated the same way as the laboratory test Larsson conducted (1977). There is no test to simulate creep implemented in the tool SoilTest and a general test was performed.

The general test function in SoilTest includes facilities to define arbitrary strains and stresses to soil sample. The test can be conducted drained or undrained. The initial stresses are chosen to simulate the in-situ stresses for the soil sample (PLAXIS, 2012). Before any creep was added to the general test it was compared with the triaxial undrained compression test also simulated by PLAXIS SoilTest. This was done by simulating the soil samples in-situ stresses and then to add a new phase that corresponds to the compression from the triaxial test to the sample, both vertical and horizontal stresses are chosen. Also the strain rate is chosen in this phase and it is chosen to 0.6 % per hour, which is the normal strain rate used in Sweden. Figure 8.20 shows stress-strain relationship for a general test (blue dashed line) and a triaxial test (red solid line) from the tool SoilTest.

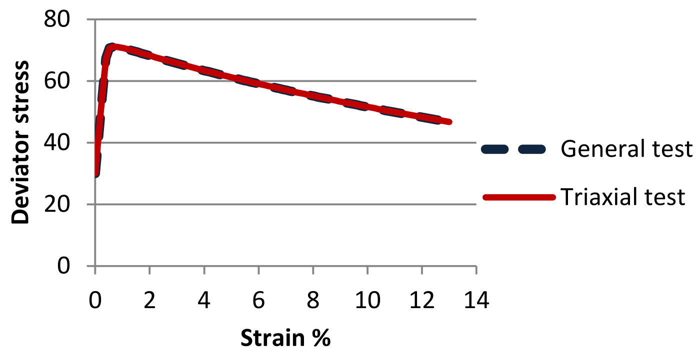

Figure 8.20. Comparison of a simulated general test and a simulated triaxial compression test from the tool SoilTest in PLAXIS.

The fit is good and shows that the general test behaves the same way as an undrained triaxial test. The general test is now used to simulate Larsson's (1977) tests for undrained creep but with parameters from parameter set 2. One phase is added to simulate the creep that the test is conducted to.

In the initial stage is the in-situ stresses applied the same way as for the undrained triaxial compression test without creep. The second phase has incremental stresses applied. This stage specifies the degree of mobilization for the soil specimen. This will be changed to correspond for three different degree of mobilization 70, 85 and 92%. The degree of mobilization was calculated from the obtained shear strength divided by the maximum undrained shear strength from the results of the undrained triaxial compression test presented in Figure 8.20. In table 8.5 input values corresponding to the three different degrees of mobilizations are presented. Values for σ'_1, σ'_3 and ε were collected from the already conducted triaxial test and the remaining values in table 8.5 were calculated from them. When the soil specimen is mobilized to the defined mobilization one more phase is added. In this phase are all stresses kept constant and the only variable is time, the time is chosen to 100 days, in this last phase creep will be evolving in the soil sample.

Table 8.5 Input values for SoilTest CK$_0$UC-creep

Mob (%)	σ'_3 [kN/m²]	σ'_1 [kN/m²]	$\Delta\sigma'_3$ [kN/m²]	$\Delta\sigma'_1$ [kN/m²]	t [day]	ε_1
42	-55.00	-84.90	0.00	0.00	0.00000	0.00%
70	-48.24	-98.41	-6.76	13.51	0.0139	0.21%
85	-44.86	-105.15	-10.14	20.25	0.0208	0.31%
92	-43.14	-108.39	-11.86	23.49	0.0243	0.36%
100	-35.83	-106.75	-19.17	21.85	0.04166	0.62%

The results from general SoilTest with creep can be seen in Figure 8.21 for parameter set 1 and Figure 8.22 for parameter set 2. With parameter set 1, one of three test had tertiary creep at a degree of mobilization of 92%, the test with lower degree of mobilization settled with time and only shown small creep strains. Parameter set 2 had none of the test in tertiary creep. This result shows large differences from the result obtained from Case 2 were several tests went to tertiary creep for a degree of mobilization of 67% and higher for parameter set 1 and for 71% and higher for parameter set 2.

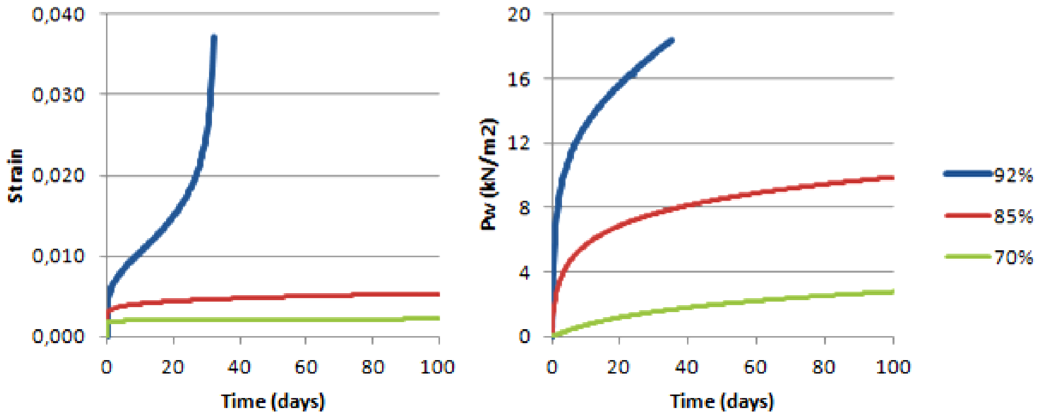

Figure 8.21 The left figure shows evolving creep in strains from a triaxial compression test generated for three different degrees of mobilization as a function of time. The figure to the right shows the generated pore water inside the specimen over time. Both diagrams are for parameter set 1.

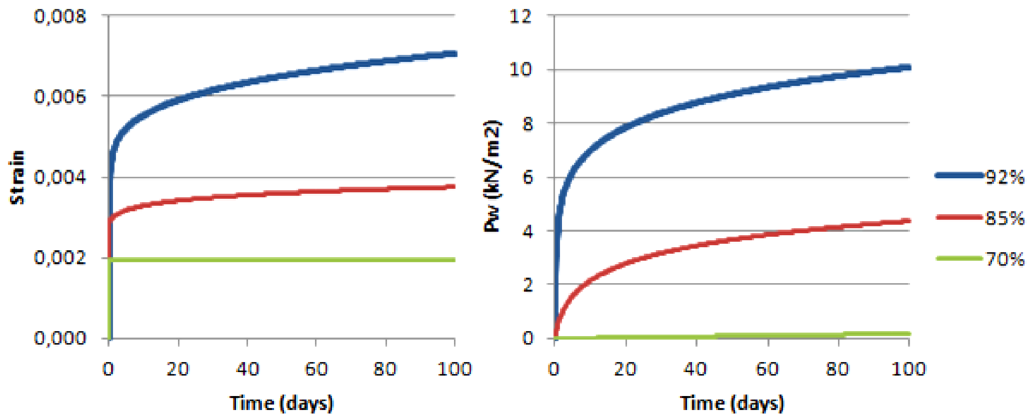

Figure 8.22 The left figure shows evolving creep in strains from a triaxial compression test generated for three different degrees of mobilization as a function of time. The figure to the right shows the generated pore water inside the specimen over time. Both diagrams are for parameter set 2.

9 Discussion

Overall Creep-SCLAY1S is able to simulate tertiary creep and to indicate on the same trend that Larsson found in his undrained creep test (1977). In this section the Hardening soil model and Creep-SCLAY1S are going to be discussed followed by results and comparisons between case one, two and three. The first two cases are shown in Figure 9.1. Both these cases were modelled in the Hardening soil model and Creep-SCLAY1S. The third case is a simulation of the tests Larsson conducted (1977) which are undrained triaxial compression tests with creep, these are simulated in the tool SoilTest in PLAXIS with Creep-SCLAy1S and not shown.

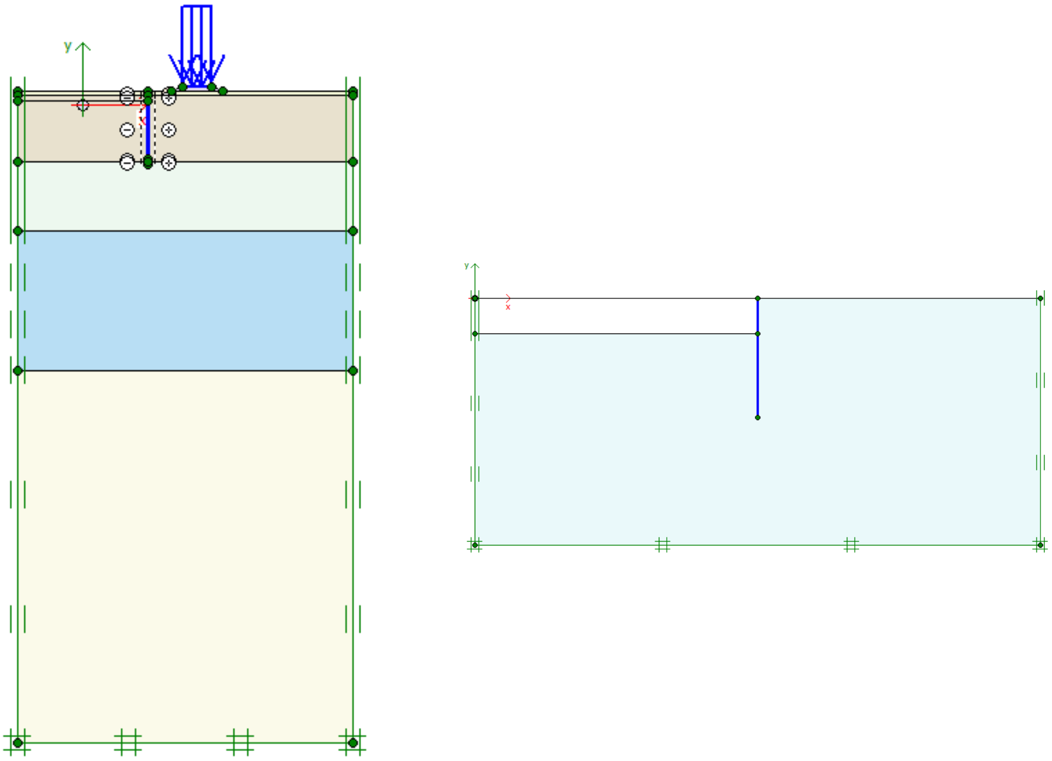

Figure 9.1 Case 1 is shown in the figure to the left and Case 2 to the right. The train load in case one is shown as arrows. Note that the scale differs between the cases.

The first case was an excavation with an embedded cantilever wall with a train load next to it. The Train load is shown as the distributed load (arrows) in the Figure 9.1. The second case is a deeper excavation with an embedded cantilever wall, but in this case the train load is removed.

9.1 The Hardening Soil model

The Hardening soil model tends to need higher stiffness parameters, than those that were measured for the soft soil, to match the laboratory tests. This shows the importance of comparing the model to laboratory data to verify that the behaviour of the soil is correct in the model. This especially due to that the model needs drained triaxial tests which are unusual to conduct and modified undrained tests are used instead. A problem with the implementation of the Hardening soil model for soft clays is the values of E_{oed}^{ref}. The problem is the error check in the program which does not allow this value to be as low as derived from the laboratory tests, however, since a good fit between laboratory test and the model is achieved, thus not considered critical.

In the second case excavation without train load, clay layer two was chosen. Unfortunately the matched parameters lead to this layer having to high shear strength, see for example in Figure 7.7. This affects the results for both the factor of safety and deformation in the excavation.

It is clear that the Hardening soil model does not account for any anisotropy and consequently it is impossible to make a good match with the triaxial extension tests. This also influences the global factor of safety which is calculated in the model because no extension strength was obtained from the extension tests. The compressive strength is higher than the extension strength and the global factor of safety becomes over predicted.

9.2 Creep-SCLAY1S

Creep-SCLAY1S is a complex model accounting for several additional factors. This makes the computation time quite long even for simple problems. This is however not noticed in the application SoilTest which works at similar speed for both models.

An advantage this model has is that the input values for extension and compression are similar. When modifying parameters with the model it is important to control ω, which accounts for the anisotropy in the soil, for simulating the extension values because the effect of this value is negligible in compression simulations. If this is not fixed, the results from Creep-SCLAY1S in extension is similar to the result from the Hardening soil model and the same over prediction should occur. Additionally, to be able to compare the parameter sets against each other, the triaxial extension and compression test should be conducted on clay from the same depth.

9.3 Case 1

It is clear that Creep-SCLAY1S is not optimal for problems like Case 1 excavation with train load. With a large static temporary load applied in this kind of models that accounts for rate-effects, the model is not capable of producing realistic results. Smaller loads that are not close to preconsolidation pressure at the surface are probably more likely to work, but if a temporary load is going to be modelled with a creep model one way of doing it might be to model pore pressures that corresponds to the true load that a train creates while passing. This could probably be done with liable pore water measurements from this kind of load. Another thing not tested in this thesis is how OCR influences the settlements. It might be that it needs to be higher than calculated from the Swedish method. The model assumes the OCR values for a 1D oedometer test. However, the stress paths are good with the OCR from the method used in Sweden and with a higher OCR they will change too. The OCR for Creep-SCLAY1S should be investigated in the future to ensure the use of the model on Scandinavian soft clays.

Another thing that need to be considered when a using a model that takes time into account is the time for every construction phase. Different time intervals give different deformation, as shown in Case 1, and this parameter needs to be considered while modelling.

Another problem that should be investigated with Case 1 is the parameter set. The geometry of the problem is relatively simple and no hard calculations are applied. The destructuration parameter was deactivated in the first case due to computation problem which came during consolidation calculations after the initial phase. In this phase there were very low pore pressures, and with a high destructuration parameter the pore pressure continued to increase and large deformations occurred in the model. Using a set of parameters that has been used for benchmarks for the model could be used to investigate if the parameter destructuration once again could be used. The parameter set that are derived in this thesis are, however, not optimal for the model.

A conclusion from Case 1 is that Creep-SCLAY1S cannot model these kinds of problem in Ultimate limit state and further research on the use of rate-dependent and how to use them for ultimate limit state should be carried out.

9.4 Case 2

The failure mechanisms were tried for both models and the same failure appear with rotation around a point located above the bottom of the sheet pile wall. The deformations from the excavation were too large for both models but not unrealistic. The Hardening Soil model has smallest deformation but if extension strength had been accounted for the results might have been closer immediately after the excavation.

A difference between the Hardening soil model and Creep-SCLAY1S that need to be considered is that no interface is installed in the latter simulations. This makes it impossible to model a gap between the wall and the soil that can be filled with water and the excavation is not approved in the Ultimate limit state according to Eurocode 7. The gap between the soil and the retaining wall got unrealistically large when interface elements were used, and hence they were deleted. This is not considered in this thesis but important for future calculations. This could also have influenced Figure 8.15 which shows the earth pressure against the retaining wall at the active side. There is a jump at the points showing the pressure after 180 days at four m depth. This could be because the clay cannot move from the wall. But it could also depend on locally errors in the mesh when looking into a structure in detail.

No consolidation is used in Case 2 because it generated strange results when an excavation was constructed. It seemed to be a mesh dependent problem with large deformation occurred inside of the excavation but it could also be problem with the boundary conditions. This problem could not be solved and all consolidation phases were deleted for this case. Because of this no consolidation are accounted for in the calculations and only rate effects is activated. The modelled case is not realistic because it is seen undrained during 180 days but then it is possible to see the trend that the creep effect has on the excavation. But then is a temporary excavation considered undrained and it is possible to model correct rate effects over shorter periods.

An advantage for this advanced model is that almost every parameter comes from laboratory test which are regular used in Sweden. However, there is one exception and that is the incremental loading test. In the investigated area no incremental stepwise oedometer test had been conducted, and these are an important parameter for Creep-SCLAY1S. The predicted ratio of λ_i^* and μ^* are very sensitive, and without correct values the creep function may produce errors. The ratio of λ_i^* and μ^* were tested in

Case 2 for two different parameter sets. The first one that was modified with an λ_i^* of 0,22 came into creep rupture 15 days after construction of the excavation while the second which had λ_i^* of 0,12 never reached tertiary creep. The calculated parameter for λ_i^* was 0.15 which shows the sensitivity of the model for this parameter. It should be noted that all input parameters were changed for the different λ_i^* to fit the stress strain behaviour of the clay. It is recommended that these tests are performed for the correct area if this model is going to be used in a project in the future.

The tertiary creep appears too early for Case 2 which could depend on the Global factor of safety calculated from the Hardening soil model. Only compressive strength is used in all calculations and smaller deformations than reality should be expected, and if the Creep-SCLAY1S works as it is supposed to, which is not tested for this thesis, passive strength should be accounted for and the over prediction should not be as large as for the Hardening soil model. Also the safety calculation used in the Hardening Soil model assumed Mohr Coulomb which has unrealistic stress paths and pore pressure which also gives an over prediction to the factor of safety. These factors together may give an over prediction as large as 33% and if that is the case than the factor of safety for Creep-SCLAY1S is on 1.1 which corresponds to a degree of mobilization on 91 % and tertiary creep should appear, which it also does for parameter set 1. The degree of mobilization is defined as the ratio between the current stress state the soil is in and the maximum undrained shear strength it can withstand. If this assumption of having an over predicted factor of safety from the Hardening Soil model parameter set 1 could be better than expected when the results were presented.

9.5 Case 3

Compared to Case, 2 tertiary creep developed later when it was tested in an undrained triaxial soil test than it did when it was tested for the excavation without train load. Only one of six tests went to tertiary creep, and this for a degree of mobilization of 92 %. These tests support the conclusion that the transition between factor of safety from the Hardening soil model and Creep-SCLAY1S may be over predicted.

There are a lot of uncertainties in the parameter sets that were tried for this thesis. Probably it would have been better to try parameters that already were tested for a benchmark project to be certain of the behaviour of the clay close to an excavation. Creep-SCLAY1S is able to show the trend that was part of the aim in this thesis and the use of it is promising. However before any further tests for excavations are performed a sensitivity analysis for parameters should be conducted and tried for more certain results.

Another thing worth mentioning is that the analysis in this thesis is based on the test Larsson conducted (1977) but these are not verified by other experiments and the limit of 80% percent may not be correct.

10 Conclusion

It has been shown that Creep-SCLAY1S models the behaviour of creep rupture fairly well at an excavation for serviceability states and presents how long time the excavation may be open until creep rupture occur, but it has also been shown in the thesis that the model is not compatible for ultimate limit states. However, the results supports that there is a need for a margin in the factor of safety to ensure that there is no creep rupture at the excavation, but Creep-SCLAY1S cannot calculate the factor of safety, because it is implemented as a user defined model in PLAXIS and not a standard, and it is uncertain how large the margin for this factor must be to avoid creep rupture.

The input parameters for the model are derived from common laboratory tests in Sweden except for the creep parameters that need an incremental loading test or several CRS-tests with different strain rates. These parameters has been shown to be sensitive to the results and are recommended to be derived from real tests and not approximated as they are in this thesis.

There are some uncertainties in the parameter sets and further research and parametric studies of Creep-SCLAY1S is recommended before it is implemented as a usual tool to analyse rate effects at excavations but the results are still promising for future use.

11 References

ArcelorMittal. (2013, 03 25). *Arcelor Mittal - Products Steel sheet piling - U sections*. Retrieved 03 25, 2013, from http://www.arcelorprojects.com/projects/europe/foundationsolutions/EN/sheet_piling/U_sections/AU14.htm

Azizi, F. (2000). *Applied analysis in geotechnics.* Great Britain: E & FN Spon.

Bardet, J.-P. (1997). *Experimental Soil Mechanics.* New Jersey: Prentice-Hall.

Brinkgreve, R., Broere, W., & Waterman, D. (2008). *PLAXIS Finite Element Code for Soil and Rock Analyses. 2D-Version 9.* Netherlands: PLAXIS NL.

Burland, J. B. (1990). On the compressibility and shear strenght of natural clays. *Geotechnique 40, No. 3* , 329-378.

Campanella, R. G., & Vaid, Y. P. (1974). Triaxial and plaine strain creep rupture of an undisturbed clay. *CDN Geotech Journal* , 1-10.

Craig, R. F. (2004). *Craig's Soil Mechanics 7th edition.* New York: Taylor & Francis.

Gourvenec, S., & Randolph, M. (2010). Consolidation beneath Circular Skirted Foundations. *International journal of Geomecanics Vol. 10* , 22-29.

Graham, J., & Houlsby, G. T. (1983). Anisotropic elasticity of a natural clay. *Geotechnique No. 2* , 165-180.

Grimstad, G., Degago, S. A., Nordal, S., & Karstunen, M. (2010). Modeling creep and rate effects in structured anisotropic soft clays. *Acta Geotechnica* , 69-81.

Havel, F. (2004). *Creep in soft soils.* Trondheim: Norwegian University of Sience and Technology.

Hinchberger, S. D., Qu, G., & Lo, K. Y. (2010). Constitutive apporach for rate-sensitive anisotropic structured clays. *International journal for numerical and analytical methods in geomechanics* , 1797-1830.

Infrastruktur, K. (2005). *En kortkurs om triaxialförsök på främst normalkonsoliderade och svagt överkonsoliderade leror.* Göteborg: Chalmers tekniska högskola 2005.

Karstunen, M., Krenn, H., Wheeler, S. J., Koskinen, M., & Zentar, R. (2005). Effect of Anisotropy and Destructuration on the Behaviour of Murro Test Embankment. *International Journal of Geomechanics* , 87-97.

Karstunen, M., Sivasithamparam, N., Brinkgreve, R. B., & Bonnier, P. G. (2013). Modelling rate-dependent behaviour of structured clays. *Proc. International Conference on Installation Effects in Geotechnical Engineering* .

Kempfert, H.-G., & Gebreselassie, B. (2006). *Excavations and Foundations in soft soils.* Springer.

Krenn, H. (2008). *Numerical modelling of embankments on soft soils.* Scotland: Ph.D. Thesis University of Strathclyde.

Kullingsjö, A. (2007). *Effects of deep excavations in soft clay on the immediate surroundings -Analysis of the possibility to predict deformations and reactions against retaining system.* Göteborg: Chalmers University of Technology.

Labuz, J. F., & Zang, A. (2012, July 3). Mohr-Coulumb failure criterion. *Rock Mechanics and Roch Engineering* , pp. 975-979.

Lambe, T. W., & Whitman, R. V. (1969). *Soil Mechanics.* United States of America: John Wiley and sons.

Larsson, R. (1977). *Basic behaviour of Scandinavian clays.* Linköping: Statens geotekniska institut.

Larsson, R. (2008). *Jords Egenskaper, Information 1.* Linköping: Statens Geotekniska institut.

Larsson, R., & Sällfors, G. (1981). Hypothetical yield envelope at stress rotation. 693-696.

Larsson, R., Bengtsson, P. E., & Eriksson, L. (1997). *Predictions of settlements of embankments on soft fine grained soils - Calculation of settlement and their course with time.* Linköping: SGI Informaion 13E.

Lefebvre, G. (1981). The long term stability of a cutting slope in an overconsolidated sensitive clay. *Canadian Geotechnical Journal* , 322-323.

Leoni, M., Karstunen, M., & Vermeer, P. A. (2008). Anisotropic creep model for soft soils. *Geotechnique 58, No. 3* , 215-226.

Leroueil, S., Tavenas, F., Brucy, F., La Rochelle, P., & Roy, M. (1979). Behaviour of destructed natural clays. *Journal of Geotechnical Engineering Division, American Society of Civil Engineers* , 759-778.

Olsson, M. (2010). *Calculation long-term settlement in soft clays - with special focus on the Gothenburg region.* Linköping: Swedish Geotechnical Institute.

PLAXIS. (2012). *PLAXIS 2D Reference Manual.* PLAXIS NL.

Plaxis. (Version 1). *Plaxis-GiD Material Models Manual.* Plaxis.

Potts, D. M., & Zdravkovic, L. (1999). *Finite element analysis in geotechnical engineering theory.* London: Thomas Telford Ltd.

Schanz, T., Vermeer, P. A., & Bonnier, P. G. (1999). *The hardening soil model: Formulation and verification.* Balkema, Rotterdam: Beyond 2000 in Computional Geotechnics.

Schoefield, A., & Wroth, P. (1968). *Critical state soil mechanics.* Berkshire: McGRAW - HILL publishing Company Limited.

Silva, V. D. (2006). *Mechanics and strength of material.* Netherlands: Springer Verlag Berlin Heidelberg.

Sivasithamparam, N. (2012). *Modelling Creep Behaviour of Soft Soils.* PLAXIS B.V. & university of Strathclyde.

Sivasithamparam, N., Karstunen, M., Brinkgreve, R. B., & Bonnier, P. G. (2013). Comparison of two anisotropic creep models at element level. *CRS Press* , 72-78.

Sällfors, G., & Andréasson, L. (1985). *Kompressionsegenskaper.* Stockholm: Statens råd för bygforskning.

Trafikverket. (2013-03-25, March 25). *BanaVäg i Väst*. Retrieved 04 10, 2013, from Trafikverket: http://www.trafikverket.se/Om-Trafikverket/Andra-sprak/English-Engelska/Railway-and-Road/Railway-Construction-Projects/BanaVag-i-Vast-Project/

Wheeler, S. J., Cudny, M., Neher, H. P., & Wiltafsky, C. (2003). *Some developments in constitutive modelling of soft clays.* Int. Workshop on Geotechnics of Soft Soils-Theory and Practice.

Wheeler, S. J., Näätänen, A., Karstunen, M., & Lojander, M. (2003). An anisotropic elastoplastic model for soft clays. *Canadian Geotechnical Journal* , 403-418.

Wood, D. M. (2004). *Geotechnical modelling.* Oxfordshire: Spon Press.

Wood, D. M. (1990). *Soil behaviour and critical state soil mechanics.* New york: Cambridge University press.

Wood, D. M., & Graham, J. (1990). Anisotropic elasticity and yielding of a natural plastic clay. *International journal of plasticity, Vol. 6* , 377-388.

Zentar, R., Karstunen, M., Wiltafafsky, C., Schweiger, H. F., & Koskinen, M. (2002). Comparison on two approaches for modelling anisotropy of soft clays. *Proc. 8th Int. Symp. on Numerical Models in Geomechanics (NUMOG VIII)* , 115-121.

12 Appendices

Appendix A

A.1 Water content for the soil in the investigated area over depth. The black lines represent the division of the soil profile.

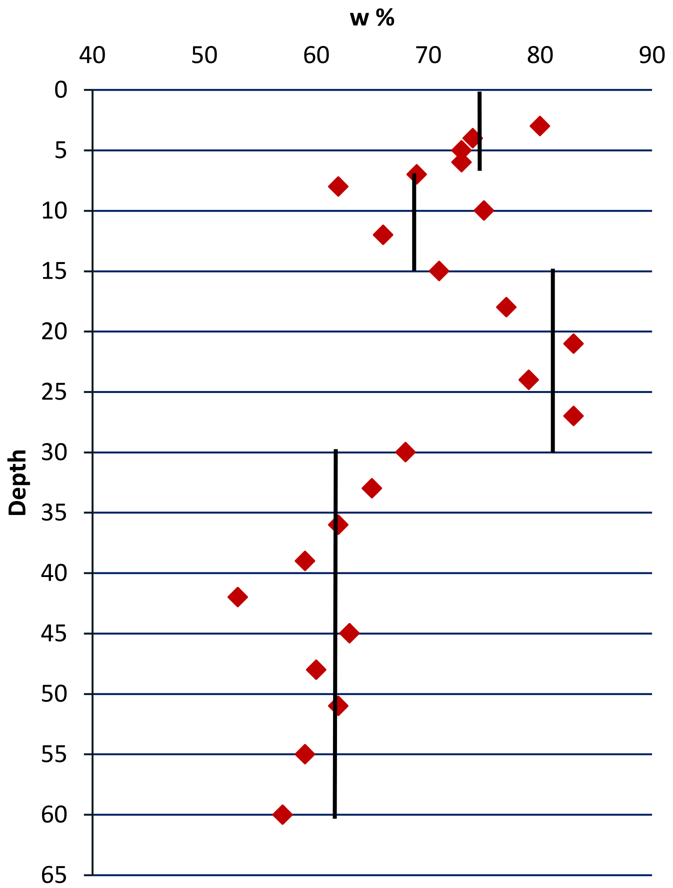

Appendix B

B.1 Input values for the Hardening Soil model

	Layer 1	Layer 2	Layer 3	Layer 4	Layer 5
γ	16	16	15.5	16.8	17
E_{50}^{ref}	7300	5600	5100	4700	4500
E_{oed}^{ref}	824	734	681	674	598
E_{ur}^{ref}	15500	22000	21600	20000	17000
m	1	1	1	1	1
ν_{ur}	0.2	0.2	0.2	0.2	0.2
c'	0	0	0	0	0
φ'	35	35	35	35	35
ψ	0	0	0	0	0
POP					
OCR	1.26	1.27	1.27	1.11	1.14
k (m/s)	2*10^-9	3*10^-10	2*10^-11	3*10^-12	3*10^-13
K_0	0.55	0.55	0.55	0.55	0.55

B.2 Modified input values for the Hardening Soil model after comparison with CK_0UC.

	Layer 1	Layer 2	Layer 3	Layer 4
γ	16	16	15.5	16.8
E_{50}^{ref}	11000	9000	9000	6000
E_{oed}^{ref}	3800	3100	3050	2100
E_{ur}^{ref}	24000	22000	20000	12000
m	1	1	1	1
mob. Shear strength	0.78	0.8	0.5	0.8
Rf	0.8	0.9	0.9	0.9
ν_{ur}	0.2	0.2	0.2	0.2
c'	0	0	0	0
φ'	35	35	35	35
ψ	0	0	0	0
POP				
OCR	1.26	1.27	1.27	1.27
k (m/s)	2*10^-9	3*10^-10	2*10^-11	3*10^-12
K_0	0.6	0.647	0.67	0.645

Appendix C

C.1 Input values for Creep-SCLAY1S

	Layer 1	Layer 2	Layer 3	Layer 4
κ^*	0.008	0.007	0.013	0.009
ν'	0.2	0.2	0.2	0.2
λ_i^*	0.15	0.15	0.15	0.15
λ^*	0.37	0.57	0.50	0.39
M_c	1.42	1.42	1.42	1.42
M_e	1.55	1.55	1.55	1.55
ω	8.06	5.19	5.97	7.67
ωd	0.96	0.96	0.96	0.96
ξ	9	9	9	9
ξd	0.2	0.2	0.2	0.2
OCR	1.26	1.26	1.27	1.11
POP				
e_0	2	1.75	2	1.7
α_0	0.55	0.55	0.55	0.55
χ_0	19	19	19	12
μ^*	0.006	0.006	0.006	0.006
τ	1	1	1	1

C.2 Modified input values for Creep-SCLAY1S after comparison with CK_0UC

	Layer 1	Layer 2	Layer 3	Layer 4
κ*	0.016	0.012	0.018	0.024
ν'	0.2	0.2	0.2	0.2
λ*	0.34	0.54	0.30	0.38
M_c	1.42	1.42	1.42	1.42
M_e	1.55	1.55	1.55	1.55
ω	13.00	25.00	13.00	27.00
ωd	0.96	0.96	0.96	0.96
ξ	9	9	9	9
ξd	0.2	0.2	0.2	0.2
OCR	1.3	1.26	1.34	1.3
POP				
e_0	2	1.75	2	1.7
α_0	0.65	0.55	0.70	0.65
χ_0	0	0	0	0
τ	1	1	1	1
μ*	0.006	0.004	0.007	0.006
K0	0.59	0.647	0.66	0.6459

C.3 Modified input values for Creep-SCLAY1S after comparison with CK_0UC

	Layer 1	Layer 2	Layer 3	Layer 4
κ*	0.014	0.011	0.011	0.007
ν'	0.2	0.2	0.2	0.2
λ_i*	0.35	0.54	0.5	0.39
M_c	1.42	1.42	1.42	1.42
M_e	1.55	1.55	1.55	1.55
ω	13.00	25.00	12.00	27.00
ωd	0.96	0.96	0.96	0.96
ξ	9	9	9	9
ξd	0.2	0.2	0.2	0.2
OCR	1.26	1.26	1.26	1.27
POP				
e_0	2	1.75	2	1.7
α_0	0.60	0.55	0.70	0.70
χ_0	0	0	0	0
μ*	0.006	0.006	0.006	0.006
τ	1	1	1	1
K0	0.62	0.64	0.64	0.695

C.4 Stress pass for CK_0UE Creep-SCLAY1S SoilTest

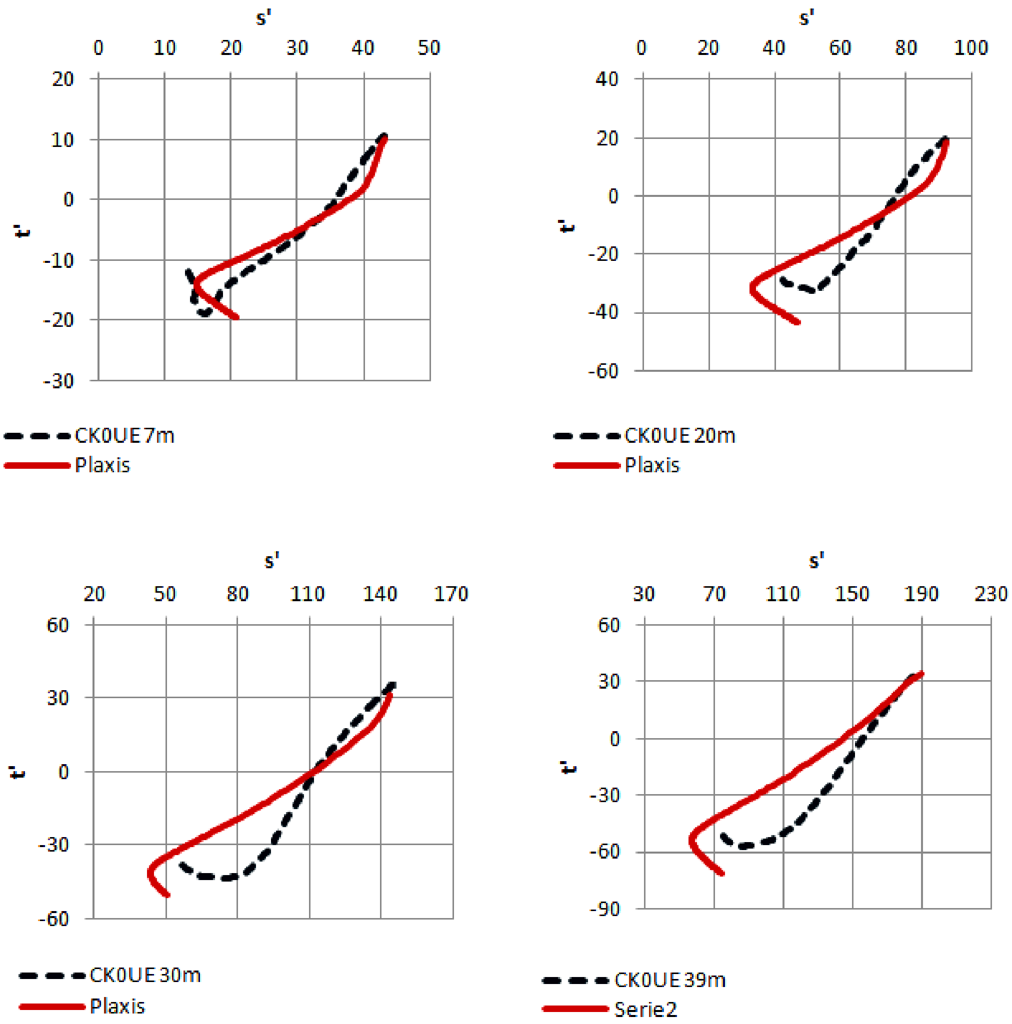

Corresponding stress paths for triaxial undrained extension tests for different depths. The blue curves are from laboratory tests and the red curves are from PLAXIS Creep-SCLAY1S user defined model.

Appendix D

D.1 Soil parameters for Fill material in the embankment

Parameter	Symbol	Fill material	Unit
Material model	Model	Mohr - Coulomb	-
Drainage type	-	Undrained	-
Weight	γ	19	kN/m
Stiffness	E	30000	kN/m2
Poisons ratio	v	0.3	-
Cohesion	c’	2	kN/m2
Friction angle	ϕ’	35	°
Dilatancy angle	Ψ	5	°

D.2 Input parameters for the sheet pile wall

Technical specification for AU14 (ArcelorMittal. 2013)

Sectional area (cm^2)	Mass/m (kg/m)	Moment of inertia (cm^4)	Elastic sectional modulus (cm^3/m)	b (mm)	h (mm)	t (mm)	s (mm)
132.3	103.8	28710	1410	750	408	10	*8.3*

Parameter	Symbol	Sheet pile wall	Unit
Material model	Model	Elastic	-
Normal stiffness	EA	2640000	kN/m2
Flexual rigidity	EI	56000	kN/m3
Weight	w	0	kN/m/m
Poisson's ratio	v	0	-

Appendix E Deformations for the Hardening soil model and Creep-SCLAy1S

Deformations after Hardening Soil model

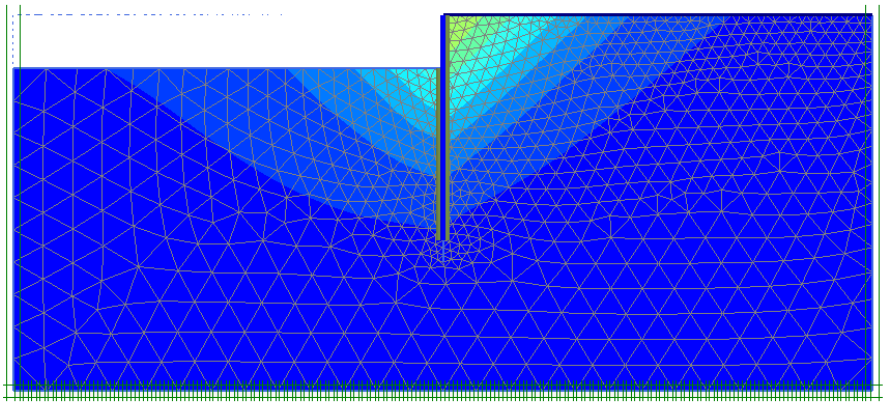

Deformations after completed excavation in Creep-SCLAY1S

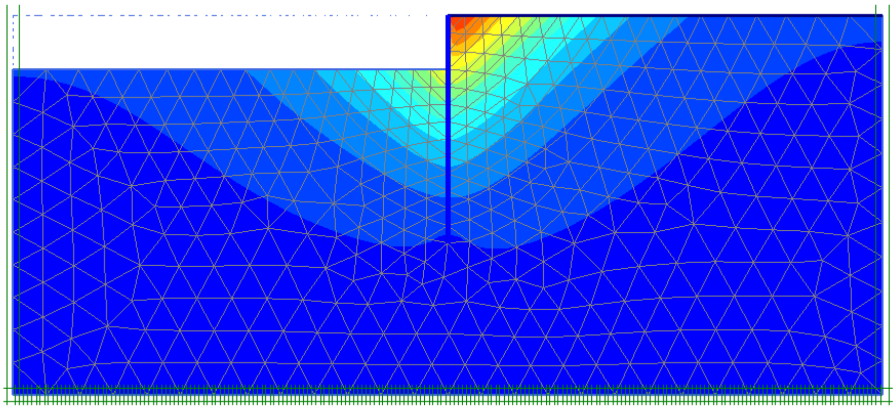

Deformations 180 days after completed excavation in Creep-SCLAY1S (Note that this has another scale than the other presented deformation)